Review

Carbon Future

Multi-atomic catalysts: Pioneering applications in the pursuit of carbon neutrality

Jiarui Yang✉ and Dingsheng Wang

Department of Chemistry, Tsinghua University, Beijing 100084, China

Cite This: *Carbon Future* **2024**, *1*, 9200019

Read Online

ABSTRACT: Since the introduction of single-atom catalysts (SACs), they have attracted considerable attention. Their high atomic efficiency and simple coordination environment make SACs a promising alternative to commercial catalysts. However, they face limitations, often showing relatively low efficiency in producing multi-carbon products. In contrast, multi-atomic catalysts (MACs), with their higher exposure of active sites, may outperform SACs owing to the synergistic effects between adjacent metallic centers. Therefore, it is essential to review the opportunities and challenges of MACs in the carbon neutrality field, offering potential guidance for future research.

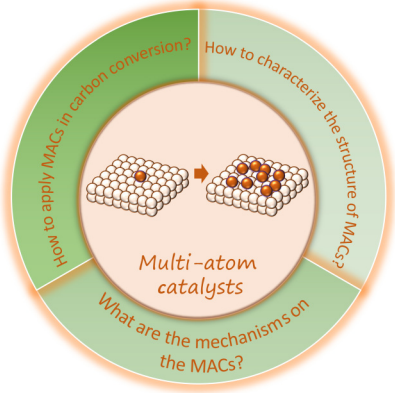

KEYWORDS: single-atom catalysts, multi-atom catalysts, electrocatalysts, carbon neutrality

1 Introduction

As global climate change and its devastating impacts become increasingly evident, the world has united around the ambitious goal of achieving carbon neutrality. This monumental challenge requires a fundamental transformation in energy production, consumption, and storage, with a primary focus on reducing greenhouse gas emissions, particularly carbon dioxide (CO_2)[1–9]. Among the numerous technologies set to drive this transition, multi-atomic catalysts (MACs), especially single-atom catalysts (SACs), stand out as potential game-changers owing to their exceptional catalytic properties and their ability to revolutionize various chemical processes.

China's commitment to peaking CO_2 emissions by 2030 and achieving carbon neutrality by 2060 underscores the immense urgency and scale of the challenge[10–17]. This national agenda requires a coordinated effort in research and development, with MACs playing a crucial role in the pursuit of clean and sustainable energy solutions[18–25].

To achieve this goal, numerous researchers have explored various approaches, employing SACs, cluster catalysts, nanoparticle catalysts, and more to enhance catalytic activity[26–32]. In addition to these catalysts, MACs offer various advantages. These systems feature isolated active metal centers composed of a few atoms, where individual metal atoms are stabilized on a supporting material[33–38]. SACs have attracted considerable attention for their unique structural and electronic properties, which lead to exceptional catalytic activity and selectivity[39–45]. These catalysts can be categorized by their elemental composition, including those derived from d-block (transition metals), ds-block (e.g., Zn, Cd, and Hg), p-block (e.g., Al, Ga, and In), and even f-block (rare earth metals) elements[46–51].

MACs offer several advantages over traditional catalysts, making them ideal candidates for carbon neutrality applications[52–57]. First, their high atomic utilization efficiency ensures that every metal atom actively participates in the catalytic process, minimizing material waste and reducing costs[58–62]. Second, MACs often demonstrate superior catalytic activity and selectivity, enabling more efficient and targeted chemical synthesis[63–70]. Third, their tunable electronic structures allow for precise control over catalytic performance, optimizing reactions for specific applications[71–79]. Finally, MACs exhibit excellent stability and durability under harsh reaction conditions, ensuring long-term reliability and operation.

Achieving carbon neutrality can be advanced by converting CO_2 into high-value products such as methane, ethylene, and ethanol[80–87]. This conversion can be achieved through thermal, photocatalytic, and electrocatalytic processes, all of which will be discussed in this review. Among these methods, electrochemical CO_2 reduction reaction (CO_2RR) stands out as a promising approach for transforming CO_2 into valuable chemicals and fuels,

Received: August 10, 2024; **Revised:** September 19, 2024
Accepted: September 23, 2024

✉Address correspondence to Jiarui Yang, yjr20.tsinghua@vip.163.com

https://doi.org/10.26599/CF.2024.9200019

thus closing the carbon cycle and helping to mitigate the effects of climate change[88–92]. The process begins with the adsorption of CO_2 molecules on the catalyst surface, followed by electron transfer and subsequent chemical transformations, resulting in products such as carbon monoxide (CO), methane (CH_4), formic acid (HCOOH), methanol (CH_3OH), ethylene (C_2H_4), and others[88–93]. MACs play a crucial role in CO_2RR by offering well-defined active sites with optimized electronic structures that facilitate CO_2 activation and the subsequent reduction steps. The unique electronic properties of MACs enhance their effectiveness in driving these reactions. Their charge states and hybridization states can be tailored to strengthen the interaction between CO_2 and the catalyst, thereby lowering the activation barrier and promoting the formation of desired products[94–99].

The products of CO_2RR mediated by MACs are diverse and offer considerable potential for various applications. For example, CO is an important feedstock for Fischer–Tropsch synthesis of hydrocarbons and the production of methanol and dimethyl ether. While CH_4 is a potent greenhouse gas, it can serve as a clean-burning fuel or be converted into other chemicals[100–103]. HCOOH, CH_3OH, and C_2H_5OH are valuable platform chemicals for synthesizing polymers, solvents, and pharmaceuticals[104–107]. The production of C_2H_4 and other higher hydrocarbons paves the way for the direct synthesis of liquid fuels and olefins, which are crucial for the chemical industry. To offer valuable insights for future research, this review will cover the characterization, applications, and mechanisms involved, as well as discuss upcoming opportunities and challenges.

2 Characterization of multi-atomic catalysts

The techniques for characterizing these catalysts are similar to those used for SACs, though there are some differences. This section will discuss both conventional and specific characterization methods for MACs, offering guidance for future research.

2.1 Conventional techniques

In this section, the conventional techniques covering morphological and structural aspects will be discussed, such as high-angle annular dark field scanning transmission electron microscopy (HAADF-STEM), X-ray photoelectron/absorption spectroscopy, and others.

First and foremost, morphological analysis is the most direct method for distinguishing a MAC system. This section will begin with a discussion of HAADF-STEM and related electron microscopy techniques. In 2021, Lu's group synthesized supported

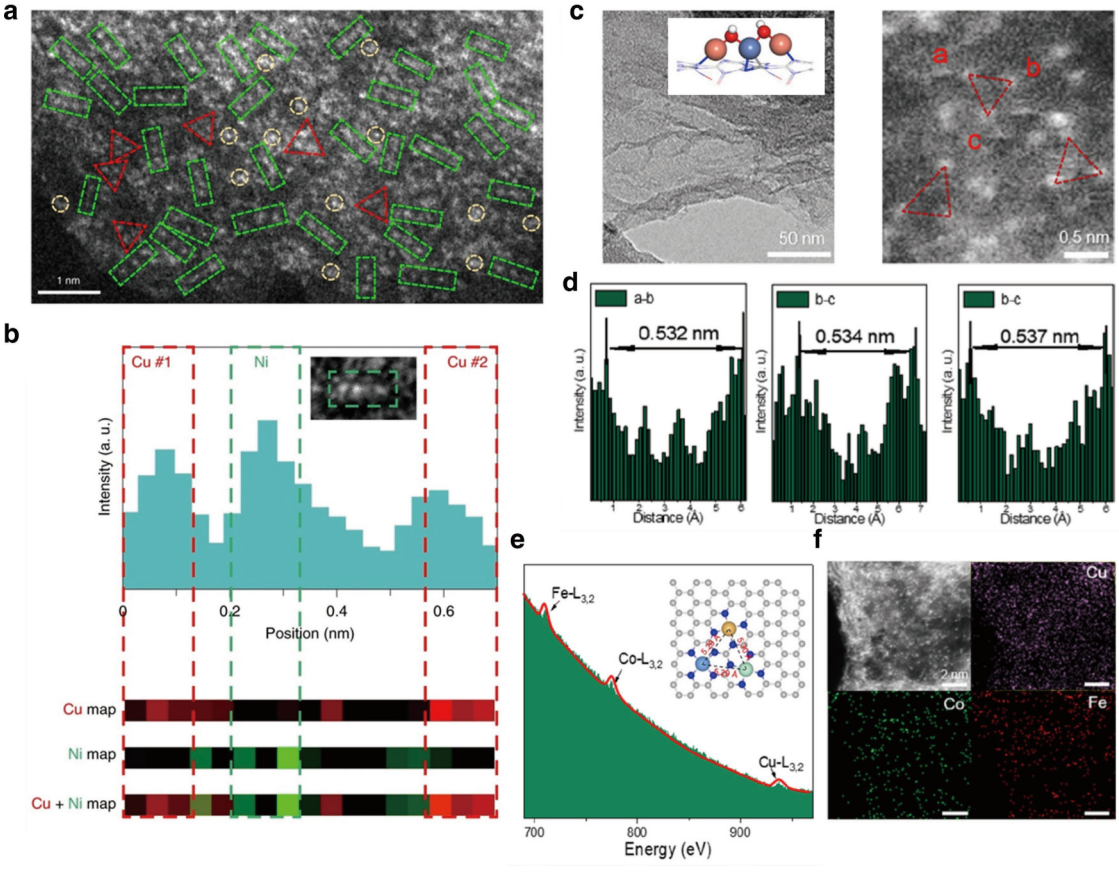

Fig. 1. The characterizations of MACs with HAADF-STEM. **a**, Representative HAADF-STEM image of Ni_1Cu_2/g-C_3N_4 captured at atomic resolution. **b**, Intensity profile and atomic-resolution electron energy-loss spectrum elemental mapping of an individual linear trimer, as shown in the inset. Reproduced with permission from Ref.[9], © Gu, J. et al. 2021. **c**, TEM image and high-resolution HAADF-STEM image of CoFeCu-TAC, with a schematic structure of the active sites presented in the inset. **d**, Intensity profiles of the three atoms labeled in (c). **e**, EELS of CoFeCu-TAC, showing 706 eV for Fe-$L_{3,2}$, 777 eV for Co-$L_{3,2}$, and 930 eV for Cu-$L_{3,2}$, with a schematic structure of the active sites shown in the inset. **f**, HAADF-STEM image and energy-dispersive X-ray spectroscopy elemental mapping of CoFeCu-TAC. Reproduced with permission from Ref.[98], © American Chemical Society 2024.

atomically dispersed catalysts featuring Ni and Cu atomic centers (1–3 atoms)[9]. As illustrated in Figs. 1a and 1b, the HAADF-STEM results reveal numerous isolated sites comprising single-atom, dual-atom, and tri-atom states. The atomic-resolution electron energy loss spectroscopy (EELS) elemental mapping of an individual linear trimer shown in the inset of Fig. 1b clarifies the elemental composition of the atoms. The location and type of atomic centers will be examined using atomic-resolution microscopy combined with EELS, a typical analytical tool. Similarly, Yang et al. performed HAADF-STEM (Fig. 1c) and EELS (Fig. 1d) to illustrate a more complex active site composed of three elements: Fe, Co, and Cu[98]. These findings are further supported by energy-dispersive X-ray spectroscopy elemental mapping at lower resolution (Figs. 1e and 1f), which confirms that the elements are well dispersed on the substrate.

The results indicate that HAADF-STEM and other high-resolution microscopy techniques are effective for analyzing MACs. However, the complexity and delicacy of *in situ* electron diffraction experiments present considerable challenges. While electron diffraction is invaluable for understanding crystal structures and phase transitions, it can be difficult to perform under operational conditions owing to the stringent environmental control required and the risk of sample damage from electron beam exposure. These constraints often make direct *in situ* electron diffraction studies impractical for MACs, particularly given their potential applications in dynamic environments or under operational conditions.

To address these challenges and further our understanding of MAC behavior under real working conditions, there is a shift toward alternative microscopic techniques that provide both high sensitivity and compatibility with *in situ* measurements. Among these, atomic force microscopy (AFM) and scanning tunneling microscopy (STM) stand out as promising options. AFM, in particular, is well-suited for studying surface morphology, roughness, and the interactions of MACs with their environment owing to its capability to image surfaces at the nanometer scale and measure local forces and properties. Conversely, STM provides even higher resolution by probing the electronic structure of materials directly, allowing for insights into the conductivity and energy states of MACs under operation.

Moreover, the emergence of probe-based microscopy techniques designed for specific applications, such as environmental AFM and electrochemical STM, has expanded the possibilities for in situ characterization. These specialized methods allow researchers to preserve the integrity of MACs while simultaneously monitoring their structural and functional properties under diverse operational conditions, including variations in temperature, pressure, and the presence of reactive species or solvents.

In conclusion, while HAADF-STEM and other high-resolution microscopies are essential for detailed structural analysis of MACs, the challenges posed by *in situ* electron diffraction highlight the need for alternative methodologies. AFM, STM, and other probe-based microscopies, with their distinct capabilities and versatility, offer viable options for investigating the behavior of MACs under working conditions. This advancement will enhance our fundamental understanding and support the development of next-generation materials.

In addition to direct observation, spectroscopy plays a crucial role in defining geometric structures, including X-ray photoelectron spectroscopy (XPS) and X-ray absorption spectroscopy (XAS). As shown in Figs. 2a–2d, Deng and coworkers synthesized a dual-atom catalyst with atomically dispersed Cu and Zn pair sites[99]. The XAS data in R space effectively reveals the coordination environment, suggesting the presence of long-range interactions between the metallic centers. This conclusion is further supported by wavelet transform simulations, which identify a prominent peak at approximately 2.3 Å in R space and around 10.5 $Å^{-1}$ in k space. This suggests that there may be interactions between the Cu and Zn sites. In this work, Peng et al. used a dual-site coordination engineering strategy to develop an efficient catalyst, Fe and Ni, supported on nitrogen-doped carbon (denoted as FeNi SAs/NC) for metal-air batteries[100]. They also used XAS to investigate geometric and electronic structures. As illustrated in Fig. 2e, the white-line peak of FeNi SAs/NC falls between that of Fe_2O_3 and FeNi NPs/NC, indicating that it possesses higher valence states than the Fe and Ni nanoparticles. The fine structure of FeNi SAs/NC was analyzed using Fourier transform extended X-ray absorption fine structure (FT-EXAFS, Fig. 2f) spectra, which reveal a prominent peak at approximately 2.4 Å. This scattering path was further examined through wavelet transform (WT, Fig. 2g), where a reflection in k space at approximately 7 $Å^{-1}$ is attributed to the Fe–Ni coordination.

By combining fitting and theoretical calculations, Fan et al. investigated the atomically dispersed Co_2-N_6 and Fe-N_4 co-structures on nitrogen-doped carbon, referred to as Co_2/Fe-N@NC[102]. Through fitting the FT-EXAFS results (Figs. 2h and 2i) for both Co and Fe K-edges, the structural details were determined.

In addition to XAS, XPS is an effective tool for testing electronic structures. Under high-vacuum conditions, any adsorbed oxygen species can be removed from the catalyst, yielding more accurate data about the valence and electrons in the outer orbitals. Duan et al. synthesized a fully exposed single-atom Pt layer catalyst on 2D mesoporous TiO_2 nanosheets, referred to as SAL Pt@mTiO_2[97]. This few-atom catalyst features a Pt cluster approximately 7 nm in size. As shown in Fig. 3a, the Pt 4f orbitals of the SAL-Pt@mTiO_2 nanosheet shifted to higher binding energy compared to the Pt nanoparticles. This indicates that the Pt sites on the SAL-Pt@mTiO_2 nanosheet are more exposed to oxygen and may be more influenced by the substrate. Owing to its sensitivity to oxygen species, XPS is effective for clarifying the coordinated oxygen atoms. Fan and coworkers introduced a catalyst featuring a dual-metal active site comprised an oxygen-bridged indium–nickel pair (referred to as InNi DS/NC)[106]. The XPS results shown in Figs. 3b and 3c allow for the evaluation of the valence states of the dual sites through the In 3d and Ni 2p orbital spectra. The oxidation state of In is approximately + 3, while that of Ni is approximately + 2 (Fig. 3d). The binding energies of the In $3d_{5/2}$ and In $3d_{3/2}$ peaks for InNi DS/NC exhibit a slight positive shift. In contrast, the Ni $2p_{3/2}$ and Ni $2p_{1/2}$ peaks shift to lower energies compared to those of Ni SA/NC, indicating an electronic interaction in the dual-atom sites. The XPS test before and after durability tests are also performed (Fig. 3e), demonstrating that it can also act as an efficient tool for stability monitoring.

XPS is a powerful analytical technique that has been extensively validated for its reliability in investigating the intricate electronic structures of materials. However, despite its many advantages, XPS has certain limitations that need to be considered. A considerable constraint is its requirement for a high-vacuum environment during operation. This stringent condition limits the applicability of XPS in studying materials under more realistic operating conditions, such as in the presence of gases or liquids, or at elevated

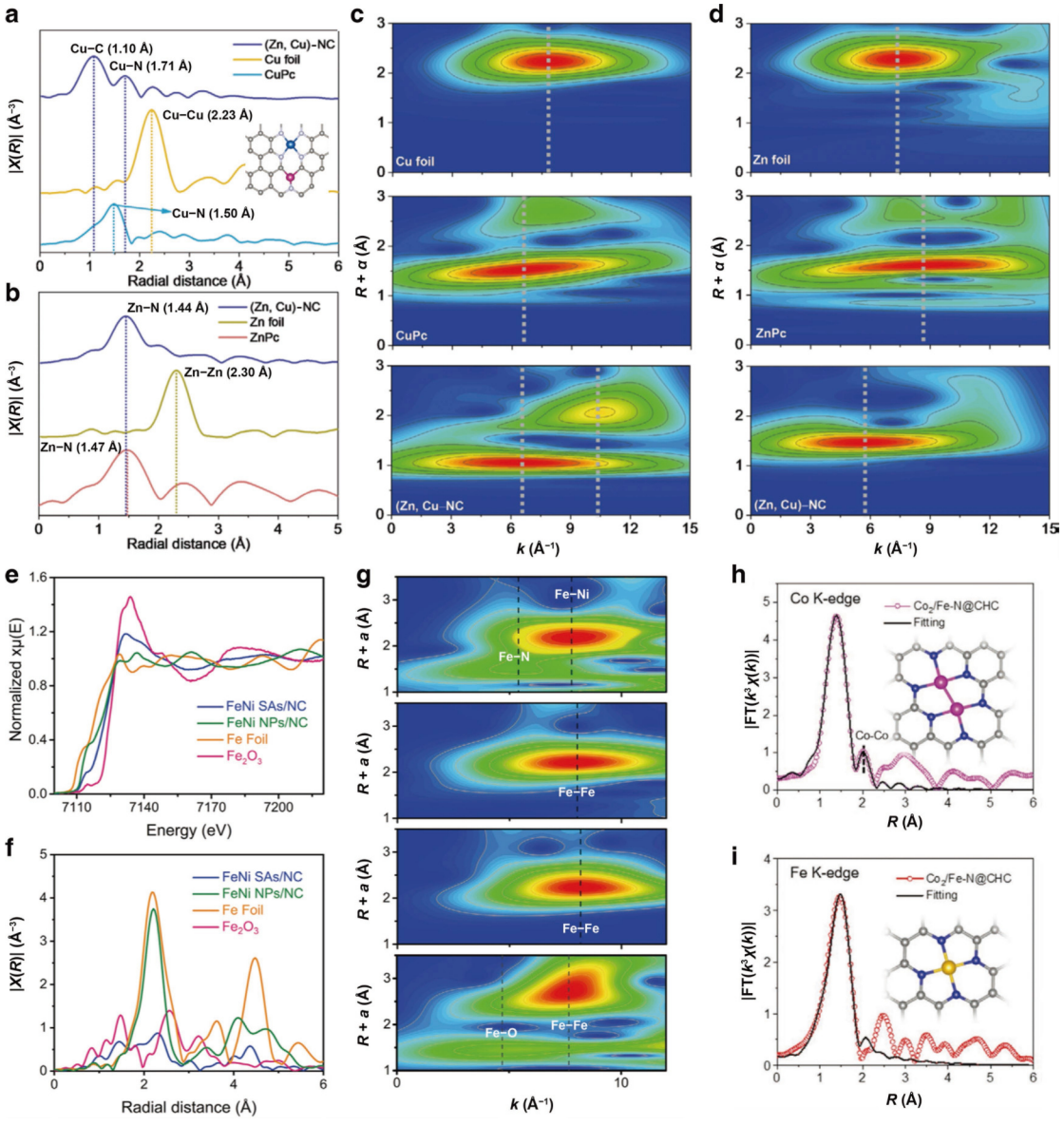

Fig. 2. The characterizations of MACs with XAS. **a**, Cu K-edge spectra for Cu foil, CuPc, and (Zn, Cu)-NC (with the structure shown in the inset). **b**, Zn K-edge spectra for Zn foil, ZnPc, and (Zn, Cu)-NC. **c**, **d**, WT-EXAFS spectra of k^3-weighted data for (c) Cu K-edge of Cu foil, CuPc, and (Zn, Cu)-NC, and (d) Zn K-edge of Zn foil, ZnPc, and (Zn, Cu)-NC. Reproduced with permission from Ref.[99], © Wiley-VCH GmbH 2022. **e**, Fe K-edge XANES spectra. **f**, **g**, FT-EXAFS spectra (f) and WT-EXAFS (g) of the Fe K-edge for FeNi SAs/NC, FeNi NPs/NC, Fe foil, and Fe_2O_3, arranged from top to bottom. Reproduced with permission from Ref.[100], © Wiley-VCH GmbH 2021. **h**, Experimental and FT-EXAFS fitting curves for Co_2/Fe-N@CHC at the Co K-edge, with the corresponding schematic model shown in the inset (Co: pink, N: blue, C: black). **i**, Experimental and FT-EXAFS fitting curves for Co_2/Fe-N@CHC at the Fe K-edge, accompanied by the corresponding schematic model in the inset (Fe: yellow, N: blue, C: black). Reproduced with permission from Ref.[102], © Wang, Z. et al. 2021.

temperatures, which are often encountered in operando or *in situ* experiments. To address this limitation, considerable efforts are being made to develop innovative techniques and enhance XPS instrumentation. For example, the integration of differential pumping systems and ultra-high-vacuum chambers has enabled the creation of microenvironments that maintain low pressure for XPS measurements while allowing the sample to be exposed to controlled gas or liquid conditions. Moreover, the exploration of ambient pressure XPS (AP-XPS) systems is a promising avenue, facilitating XPS measurements directly in air or other gases, thereby considerably expanding the range of applicable samples and conditions. Moreover, the treatment and preparation of samples for XPS analysis, especially when dealing with liquid layers or complex reaction environments, requires innovative methods to reduce interference and ensure accurate data acquisition. This involves creating specialized sample holders, employing thin film deposition techniques, and implementing surface cleaning protocols designed for specific experiments.

In conclusion, conventional characterization methods for MACs are well-established and systematic, allowing for rapid identification of these materials. However, these techniques often focus on either large areas (such as XAS) or small areas (such as HAADF-STEM), which may limit their ability to provide sufficiently accurate information about the materials. Therefore, there is a need for the development of more advanced techniques, particularly those performed under i*n situ* or operandoconditions.

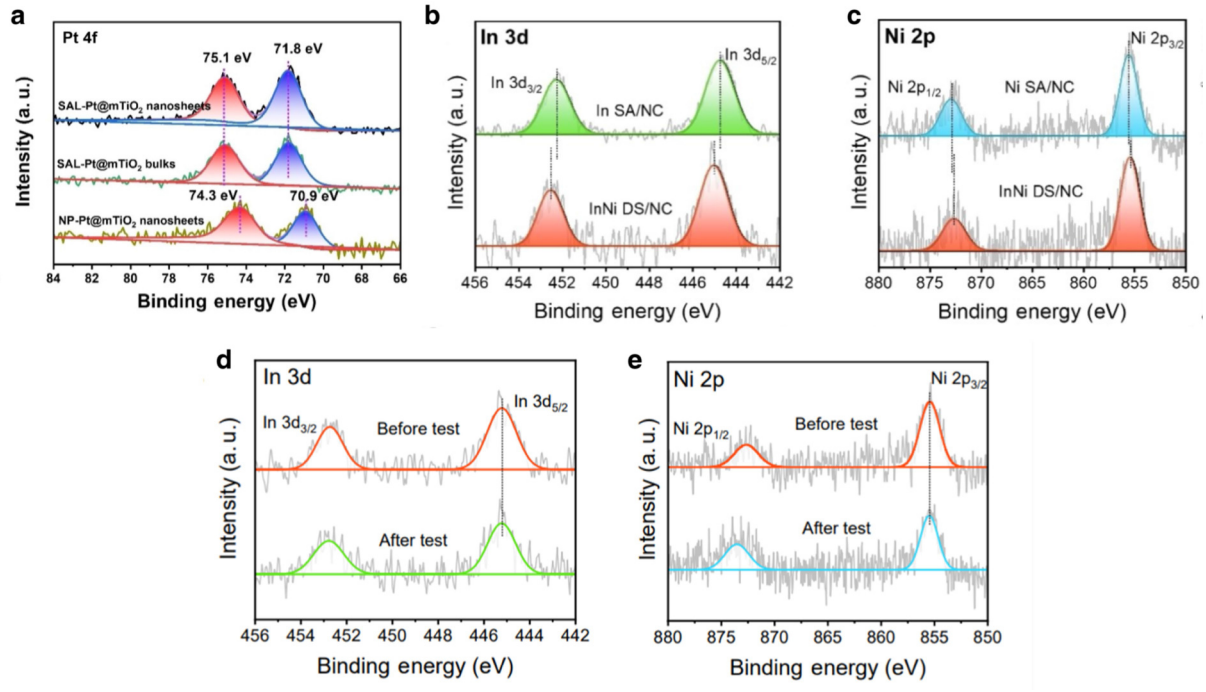

Fig. 3. The characterizations of MACs with XPS. **a**, The Pt 4f level XPS spectra of SALPt@mTiO$_2$ nanosheets. Reproduced with permission from Ref.[97], © Wiley-VCH GmbH 2022. **b**, **c**, High-resolution XPS spectra of In 3d (b) and Ni 2p (c). **d**, High-resolution XPS spectra of In 3d before and after the reaction. **e**, High-resolution XPS spectra of Ni 2p before and after the reaction. Reproduced with permission from Ref.[106], © Wiley-VCH GmbH 2022.

2.2 Specific techniques

In addition, to the conventional techniques mentioned, there are specific characterization methods for MACs that take into account the unique quantum effects present among these metallic centers.

The abovementioned methodologies, such as HAADF-STEM and XAS, are regarded as powerful tools that work together to reveal the ambient conditions and electronic configurations of multi-atom cluster catalysts, suggesting the potential for complex interactions. Additionally, a range of alternative techniques that can elucidate these properties is also recognized. Notably, single-crystal X-ray diffraction (SC-XRD) is a non-invasive and widely used method for uncovering the intricate structures of pristine, single-crystalline materials. The collected data undergoes thorough analysis and refinement, resulting in a detailed depiction of structural parameters, including unit cell dimensions, bond lengths, and angles, among others. For multi-atom clusters derived from carefully synthesized MOFs and organic ligands, SC-XRD provides a dependable method for obtaining structural insights. Electron paramagnetic resonance (EPR), with its remarkable sensitivity to unpaired electrons, is a valuable tool for determining the orbital occupancy of transition metals. Additionally, Mössbauer spectroscopy plays a crucial role in distinguishing valence states, coordination environments, and electronic properties, with increasing efforts focused on its application in the study of multi-atom clusters.

Together, the characterization techniques described above form a strong foundation for gaining deep insights into these materials. By combining these experimental results with theoretical frameworks, a more nuanced investigation of the underlying mechanisms can be achieved. However, it is essential to recognize that these measurements are generally performed *ex situ*, highlighting the need for future efforts to incorporate *in situ* methodologies that can capture the dynamic behavior of multi-atom cluster catalysts in their operational environments.

It can be concluded from previous research that the characterization of MACs has reached a high level of sophistication. However, the lack of portable and operando techniques remains a considerable limitation, hindering further development and adoption of MACs. This issue must be addressed and will be discussed in the mechanisms section.

3 Application in CO_2 conversion

The conversion of CO_2 can be achieved through various energy fields, including electrical, photonic, and thermal methods, to break C=O bonds and generate further products. The products of CO_2 conversion can be categorized into two types: single-carbon and multi-carbon products. One of the advantages of MACs is their potential to achieve high selectivity for valuable multi-carbon products. In this section, we will summarize the efforts related to both types of production and propose promising strategies for catalyst design in these areas.

3.1 Single-carbon product

Single-carbon products include CO, CH_3OH, CH_4, and various other essential chemicals that are relatively easy to synthesize but vital for industrial production. Over the past few years, substantial research has focused on the conversion of these single-carbon products, achieving efficiencies comparable to industrial standards. The primary elements used in CO_2 conversion are Au, Ag, Cu, and others, which can be classified into noble and non-noble categories.

Noble metal species have shown strong performance in the hydrogen evolution reaction, which competes with CO_2 reduction and can hinder catalyst selectivity. However, these noble metals can also enhance the hydrogeneration process and improve reactant adsorption. Therefore, achieving a balance between activity and selectivity is essential. Zhang et al. developed a diatomic Pd catalyst

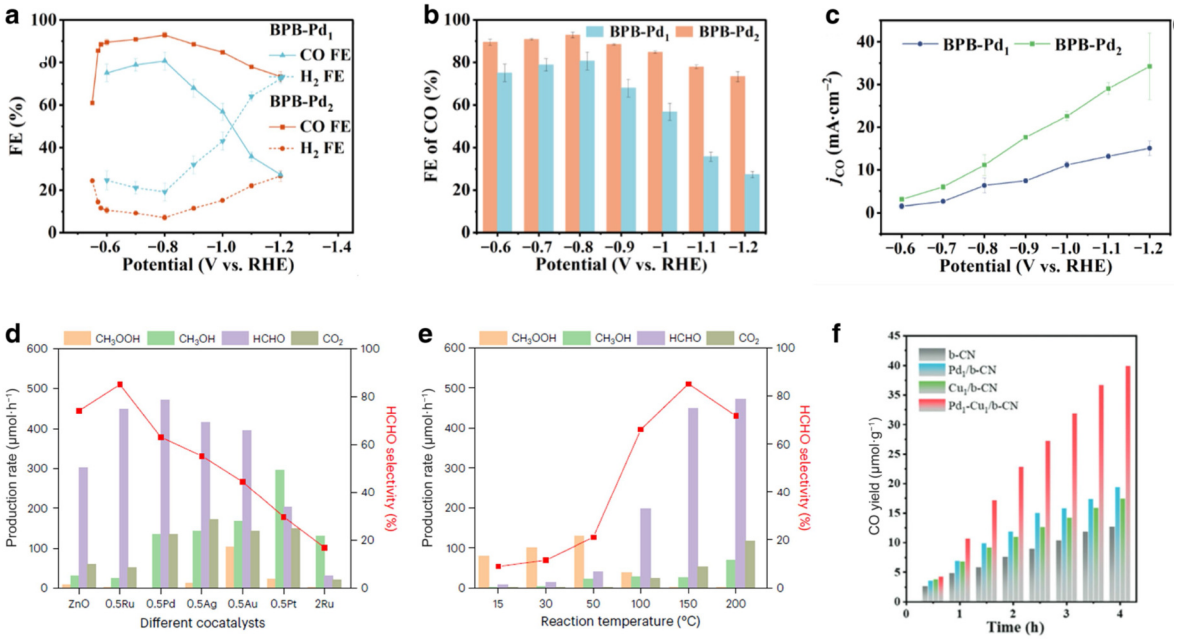

Fig. 4. The electrochemical performance of MACs towards single-carbon product. **a**, Faradaic efficiency of BPB-Pd_1 and BPB-Pd_2. **b**, Faradaic efficiency for CO production of BPB-Pd_1 and BPB-Pd_2. **c**, Geometric CO partial current density of BPB-Pd1 and BPB-Pd_2. Reproduced with permission from Ref.[108], © Tsinghua University Press 2024. **d**, Production rate of methane oxidation products over various cocatalyst-loaded ZnO species and their selectivity for HCHO at 150 °C. **e**, Effect of reaction temperature on the production rate and selectivity of HCHO over 0.5Ru-ZnO. Reproduced with permission from Ref.[109], © Xu, Y. et al. 2024. **f**, CO yield as a function of time for different photocatalysts. Reproduced with permission from Ref.[110], © Wiley-VCH GmbH 2023.

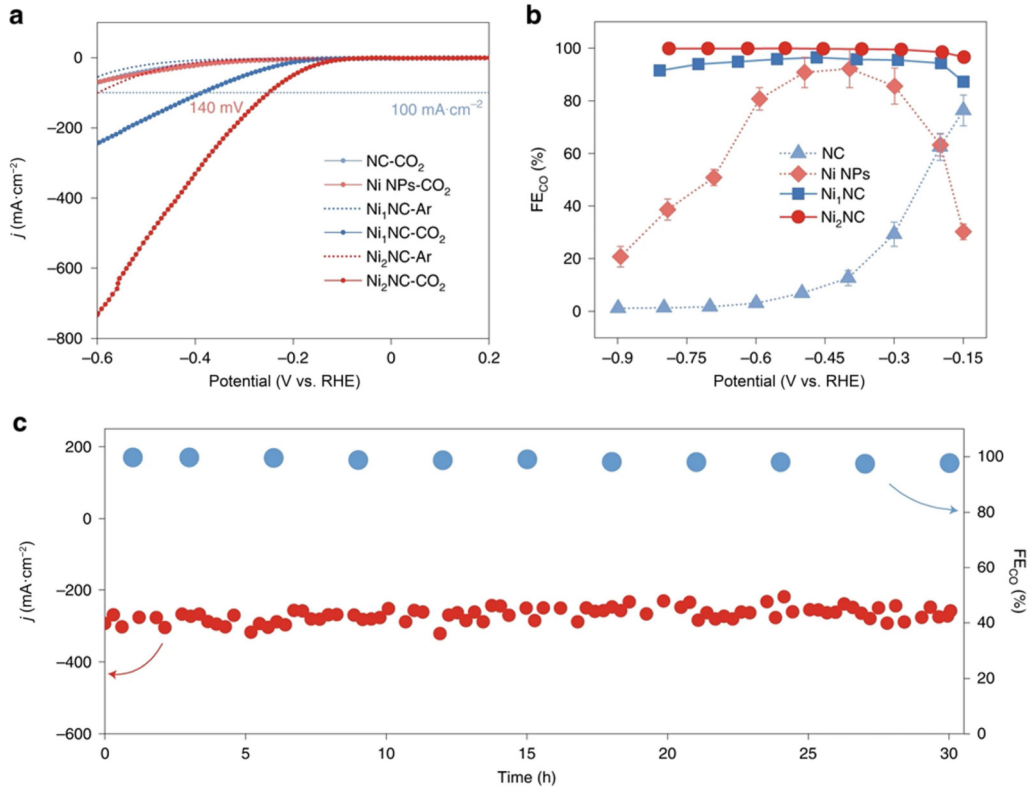

Fig. 5. The electrochemical performance of MACs towards single-carbon product. Electrocatalytic CO_2 activity was assessed using a flow cell with a 1 M KOH electrolyte. **a**, Linear sweep voltammetry curves for Ni_2NC, Ni_1NC, Ni NPs, and NC under CO_2 and Ar atmospheres. **b**, Faradaic efficiency of CO for Ni_2NC, Ni_1NC, Ni NPs, and NC. **c**, Long-term stability of Ni_2NC during electrocatalytic CO_2 reduction at −0.37 V vs. RHE. Reproduced with permission from Ref.[111], © Hao, Q. et al. 2022.

(referred to as BPB-Pd_2), which achieved a Faradaic efficiency (FE) of approximately 94.4% for CO production, owing to the synergistic effect between the dual Pd sites (Figs. 4a–4c)[108]. It is important to note that MACs can also be formed by loading isolated sites onto metallic compounds. Tang's group has made considerable contributions to this area. For example, they developed a Ru-decorated ZnO catalyst that achieved up to 90.4% selectivity for formaldehyde at 150 °C (Figs. 4d and 4e)[109].

To date, MACs, particularly dual-atom catalysts, are typically structured in a planar configuration, meaning that the two metallic centers are arranged in a 2D plane. This presents the opportunity for 3D construction as an attractive strategy for further MAC design. Yue et al. proposed a catalyst featuring in-plane Pd and interplanar Cu sites for the CO_2 photocatalytic process, successfully producing CH_4 and CO (Fig. 4f)[110]. Additionally, femtosecond time-resolved transient absorption (fs-TA) spectroscopy revealed that the charge decay lifetime of the in-plane Pd is 95.6 ps, considerably longer than that of the interplanar Cu, which is only 3.07 ps. This suggests that the in-plane Pd plays a key role in supplying electrons to the reactants and the neighboring Cu sites during the reaction.

Non-noble metal elements have also proven to be effective in CO_2RR. Among these, nickel stands out owing to its high selectivity for CO. Researchers are curious about the potential changes that dual Ni sites may bring. Zhang et al. synthesized MACs featuring dual Ni sites supported by nitrogen-doped carbon, referred to as Ni_2NC, alongside a single-atom variant named Ni_1NC[111]. The Ni_2NC catalyst demonstrates approximately 100% selectivity for CO at a current density of up to 1200 mA·cm^{-2} (Figs. 5a and 5b), indicating considerable potential for industrial applications. Furthermore, it exhibits impressive stability, maintaining performance for over 30 h at high current density (Fig. 5c). This outperforms Ni-based SACs, demonstrating the reliability of MACs. Building on the dual Ni sites, chemists have introduced heteroatoms into the system, leading to new types of MACs. Pan et al. incorporated Co and Ni dual sites in CO_2RR, achieving a maximum efficiency of 97.7% for CO production (Figs. 6a and 6b)[112]. Theoretical calculations indicate that the Co–Ni pair sites considerably enhance the formation of *COOH intermediates, thereby accelerating the reaction compared to other catalyst types.

In addition, to nickel, copper has also been extensively studied in CO_2RR. Jiao and co-workers developed asymmetric dual-atom catalysts for CO_2 reduction featuring TeN_2 and CuN_3 sites (Fig. 6c)[113]. Unlike traditional M–N–C SACs (e.g., M = Fe, Co, Ni, Cu, and Zn), the Te center activates CO_2, while the Cu center facilitates the dissociation of H_2O, thereby enhancing the CO_2RR process through a synergistic mechanism.

In the design and synthesis of SACs, particularly the typical M–N–C catalysts, one of the most important approaches is the spatial configuration facilitated by ZIF-8. Following the heat treatment process, residual zinc species remain, serving as anchor sites for the construction of dual-atom sites. Chen's group introduced a yolk–shell strategy to create a manganese and zinc

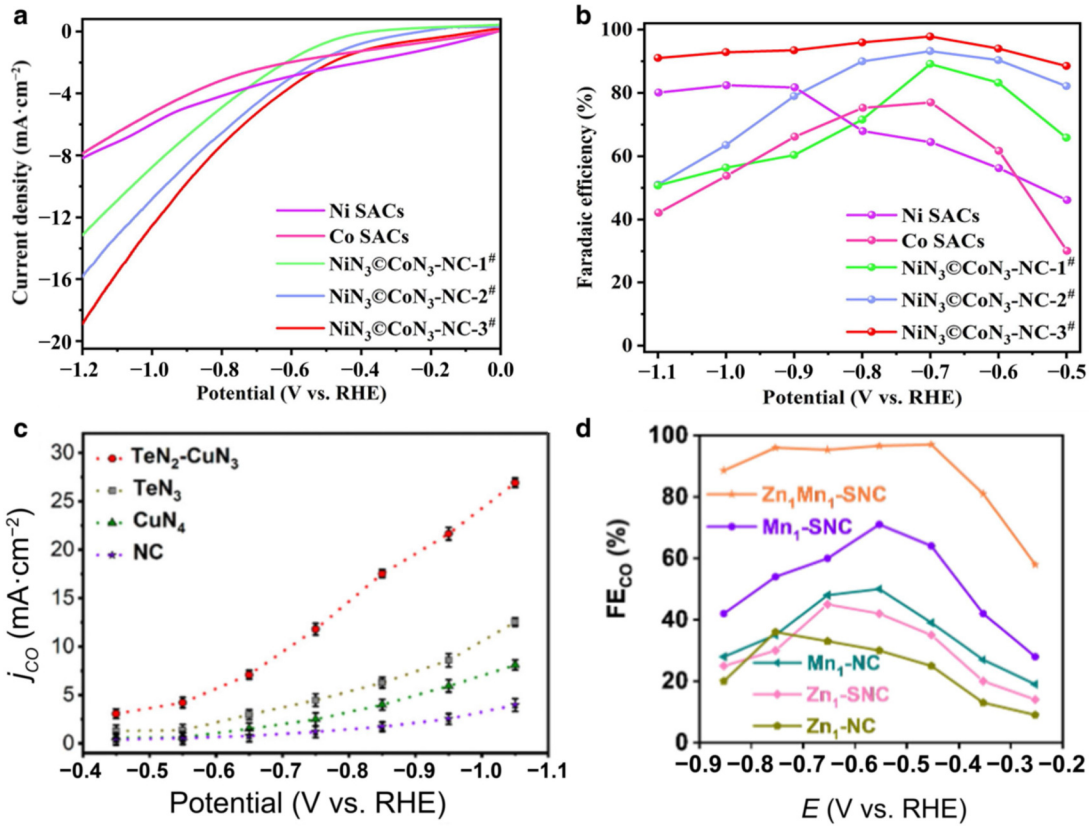

Fig. 6. The electrochemical performance of MACs towards multi-carbon product. **a**, Linear sweep voltammetry curves in a CO_2-saturated 0.1 M $KHCO_3$ electrolyte, recorded at a scan rate of 10 mV·s^{-1}. **b**, Faradaic efficiency of CO as a function of applied potentials (V vs. RHE). Reproduced with permission from Ref.[112], © Science Press and Dalian Institute of Chemical Physics, Chinese Academy of Sciences 2023. **c**, CO current density (j_{CO}) for various samples at different applied potentials (V vs. RHE), with error bars representing standard deviations. Reproduced with permission from Ref.[113], © Jiao, J. et al. 2022. **d**, FE_{CO} of the indicated catalysts. Reproduced with permission from Ref.[114], © Wiley-VCH GmbH 2023.

pair site, achieving nearly 100% selectivity toward CO and presenting a promising avenue for MAC design (Fig. 6d)[114].

The results indicate that both noble and non-noble metal-based MACs can demonstrate high catalytic efficiency for single-carbon products. If the high conversion properties of noble metal sites can be combined with the high selectivity of non-noble sites, industrial-level CO_2 conversion could be achieved in the near future.

3.2 Multi-carbon product

In addition to single-carbon products, multi-carbon products such as C_2H_5OH, CH_3COOH, and C_2H_4 are of greater value. However, many copper-based materials display high overpotential and low current density during reduction, leading to increased energy consumption and hindering their commercialization. Therefore, investigating new advanced electrochemical catalysts for the production of C_2 products is a topic of considerable scientific interest.

Building on their experience with copper-based materials, researchers initially investigated multi-atom copper or heteroatom (Cu + M) catalysts. Chen's group first proposed a single copper atom supported by a nitrogen-doped carbon substrate (referred to as Cu-SA/NPS) for CO_2RR[115]. This catalyst demonstrates a maximum selectivity of approximately 40% toward CH_3COCH_3 (Fig. 7a). Calculations indicate that the surrounding nitrogen atoms are crucial in the C–C coupling step, offering valuable insights for the future design of MACs (Fig. 7b). Subsequently, Shao et al. presented an example of MACs featuring dimer Cu units supported by boron-imidazolate nanosheets (designated as BIF-102NSs, BIF-103NSs, and BIF-104NSs), which exhibited promising Faradaic efficiency toward C_2H_4 production (Figs. 7c and 7d)[116]. Building on this approach, Xu's group incorporated additional sites into the system using closely spaced copper atoms, achieving a FE of up to 91% for ethanol production (Fig. 7e)[117]. Theoretical calculations and operando XAS results indicated that multicopper sites were formed *in situ* during the reaction. The critical function of single-atom Cu lies in controlling the formation of active sites and enhancing catalytic performance after activation. The findings suggest that surface hydroxyl groups play a crucial role in modulating the interaction between copper centers and carbon substrates. Sun et al. introduced an atomic printing strategy to create dual copper sites, achieving a FE of up to 71.7% for C_2H_4 production during CO_2 reduction. This enhancement is attributed to improved *CO adsorption and dimerization[118]. This prompts a reevaluation of previous work involving isolated Cu sites in multi-carbon production, where in situ changes in active sites may also occur. Beyond the copper system, examples of multi-carbon conversion remain limited, highlighting the need for greater focus on this important area of research.

In addition to CO_2 reduction, converting other single-carbon reactants is also an attractive strategy for achieving high selectivity toward multi-carbon products. The research indicates that the conversion of CO_2 to CO is typically the initial step in the CO_2 reduction process, and this step is well-established and relatively straightforward to achieve. Consequently, it is logical to consider combining these reactions to enhance selectivity for multi-carbon products. Building on this idea, some researchers have begun to explore this approach. Yang et al. employed several copper atomic sites supported by CeO_2 for CO electroreduction, achieving over 50% FE toward acetate across a broad current density range of 50–150 $mA{\cdot}cm^{-2}$ (Figs. 8a–8c)[119]. In addition, to experimental analysis, theoretical calculations were performed to gain a deeper understanding of the mechanism for forming multi-carbon products from CO. Kour et al. investigated a model of a conjoined-twin porphyrin-based complex in the ethanol formation process (Figs. 8d and 8e)[120]. Each of the complexes contains two metal sites

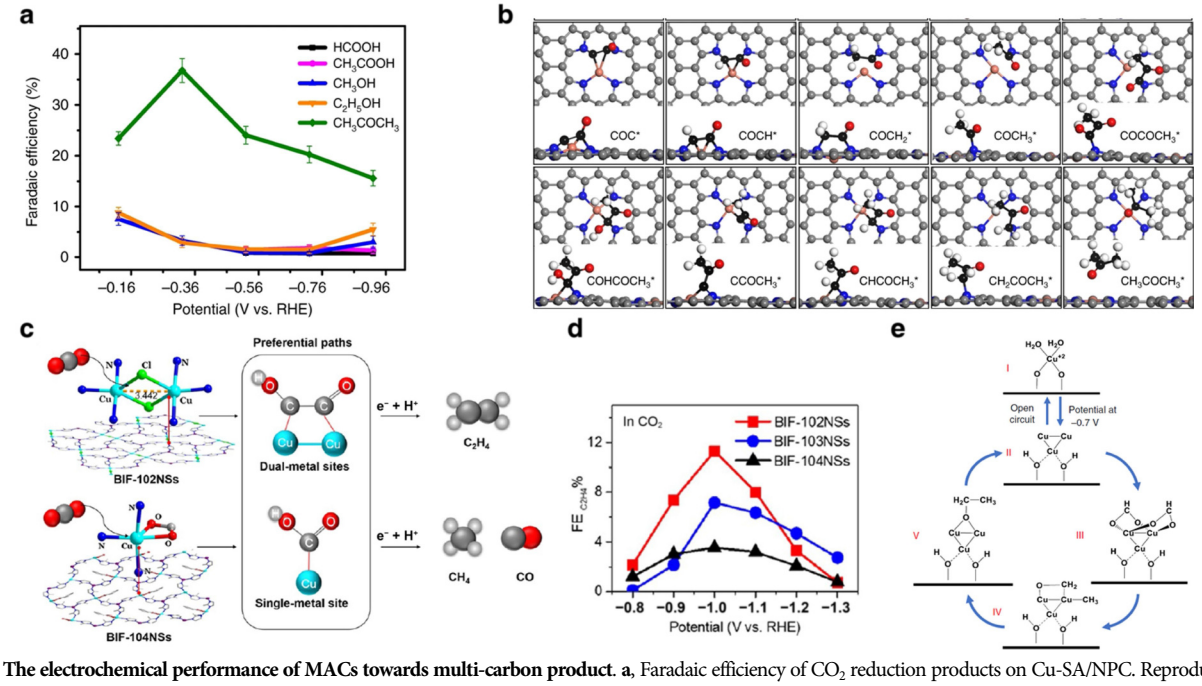

Fig. 7. The electrochemical performance of MACs towards multi-carbon product. **a**, Faradaic efficiency of CO_2 reduction products on Cu-SA/NPC. Reproduced with permission from Ref.[115], © Zhao, K. et al. 2024. **b**, Optimized structures of all reaction intermediates involved in the CO_2 reduction pathways on the Cu-pyrrolic-N_4 site. **c**, Coordination environments of BIF-102NSs and BIF-104NSs, along with an illustration of the preferential reaction pathways for different model systems. **d**, $FE_{C_2H_4}$ of electrocatalysts at various applied potentials (V vs. RHE) in CO_2-saturated electrolyte. Reproduced with permission from Ref.[116], © Wiley-VCH GmbH 2021. **e**, Proposed reaction mechanism based on operando measurements. Reproduced with permission from Ref.[117], © Xu, H. et al. 2020.

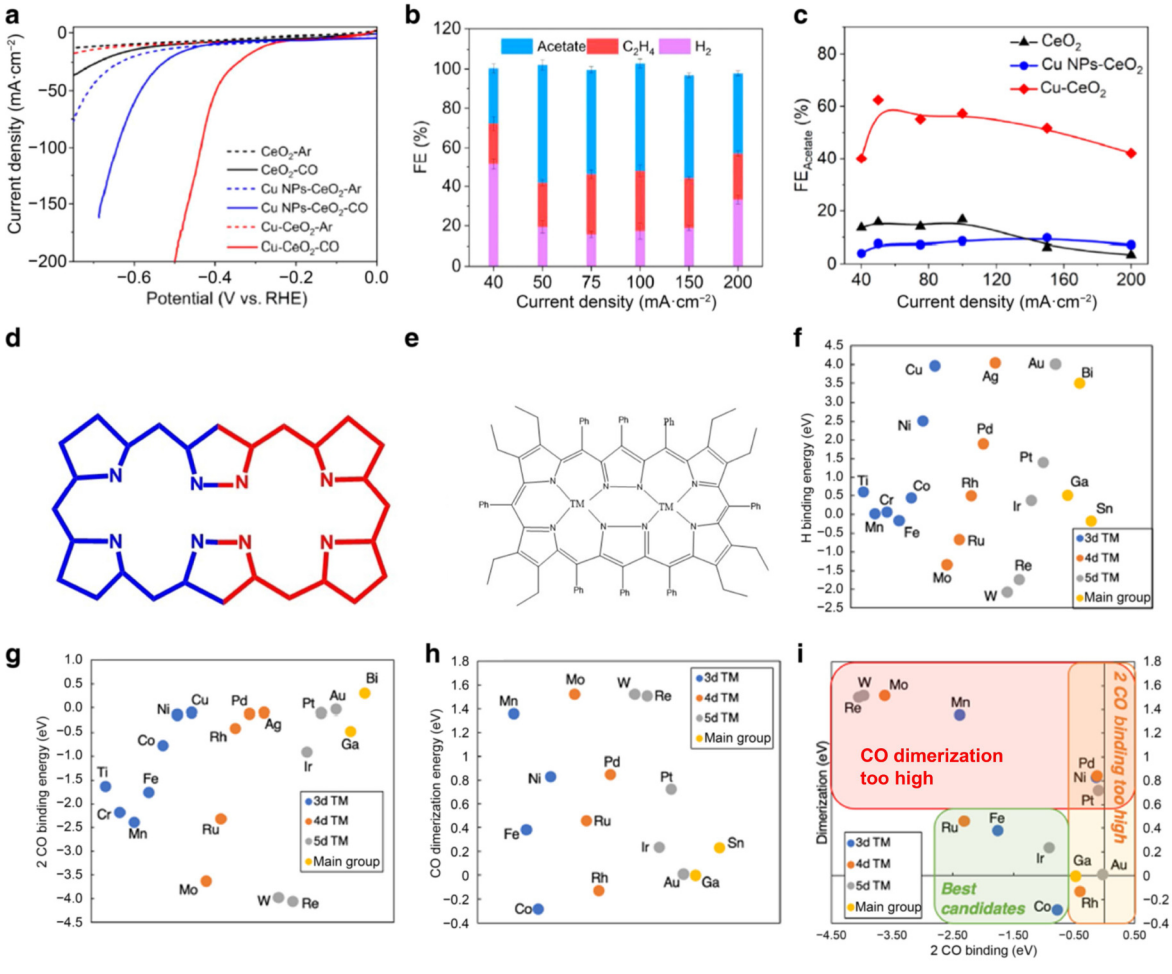

Fig. 8. The electrochemical performance of MACs towards multi-carbon product from CO reduction. **a**, Linear sweep voltammetry curves for the indicated samples. **b**, Faradaic efficiencies of products on Cu-CeO_2, with error bars representing the standard deviation from three independent experiments. **c**, FEs of acetate for CO reduction over various samples. Reproduced with permission from Ref.[119], © American Chemical Society 2023. **d**, The electronic structure of the molecule. **e**, Transition metal (TM) compound, TM_2L (TM = Co, Ni, and Cu). Reproduced with permission from Ref.[120], © Wiley-VCH GmbH 2021. **f**, H binding energies at 298.15 K (in eV) for the 20 screened elements. **g**, 2 CO binding energies at 298.15 K (in eV) for the same elements. **h**, CO dimerization energies at 298.15 K (in eV) for the 20 screened elements. **i**, Comparison of CO binding energies versus CO dimerization energies. Reproduced with permission from Ref.[121], © Elsevier Ltd. 2023.

coordinated with four nitrogen atoms. The metal centers examined in this study include Cu_2, Co_2, Ni_2, and CoNi sites. Among these, Co_2 and CoNi sites exhibit promising energy barriers for the targeted product, with low potentials of −0.59 and −0.61 V vs. RHE, respectively. The rate-determining step in the CO reduction process is the CO-CO dimerization step, a finding supported by another research. Charles B. Musgrave III and colleagues studied a range of dual-atom catalysts comprising 3d, 4d, 5d, and main group metal elements to systematically understand the properties of metallic centers during key steps in CO reduction[121]. As illustrated in Figs. 8f–8i, the CO dimerization process on Co, Rh, Au, and Ga occurs spontaneously, with energy barriers below zero. Along with the H binding energy and two CO binding energies, they identified several elements with promising potential that demonstrate high efficiency in CO reduction to ethylene, which will be further investigated experimentally in the future.

However, this is not the ultimate goal; researchers are exploring whether non-metal species can achieve efficient multi-carbon production. Hao et al. performed a theoretical analysis using a model of tricoordinated B atoms supported by C_3N_4 for their study (Figs. 9a–9c)[122]. Through sophisticated electron "accept-donation" analysis, they demonstrated that the unique tricoordinated B atoms in B_4@g-C_3N_4 exhibited a mild binding affinity toward CO, surpassing both metallic sites and bicoordinated B counterparts (Fig. 9d). This favorable interaction considerably reduces the free energy barrier for the direct dimerization of CO to just 0.18 eV. Moreover, the limiting voltage needed for the complete reduction of CO to CH_3CH_2OH is remarkably low at −0.19 V (Fig. 9e), outperforming recently reported metal-based catalysts such as Cu_4-$C_5N_2H_2$ and Cu_2Zn_2-$C_5N_2H_2$. These findings not only support the concept of a metal-free electrocatalyst for CO reduction to ethanol but also pave the way for future research in this area. By establishing a theoretical foundation, they make a considerable contribution to the pursuit of sustainable carbon neutrality goals, presenting a promising alternative to traditional metal-based catalysts.

In conclusion, extensive research has been performed on both single-carbon and multi-carbon products. However, achieving high durability—extending to thousands of hours—for multi-carbon products catalyzed by non-copper multi-atom catalysts at industrial rates remains a formidable challenge and a major barrier in this field. Therefore, considerable efforts should be focused on this

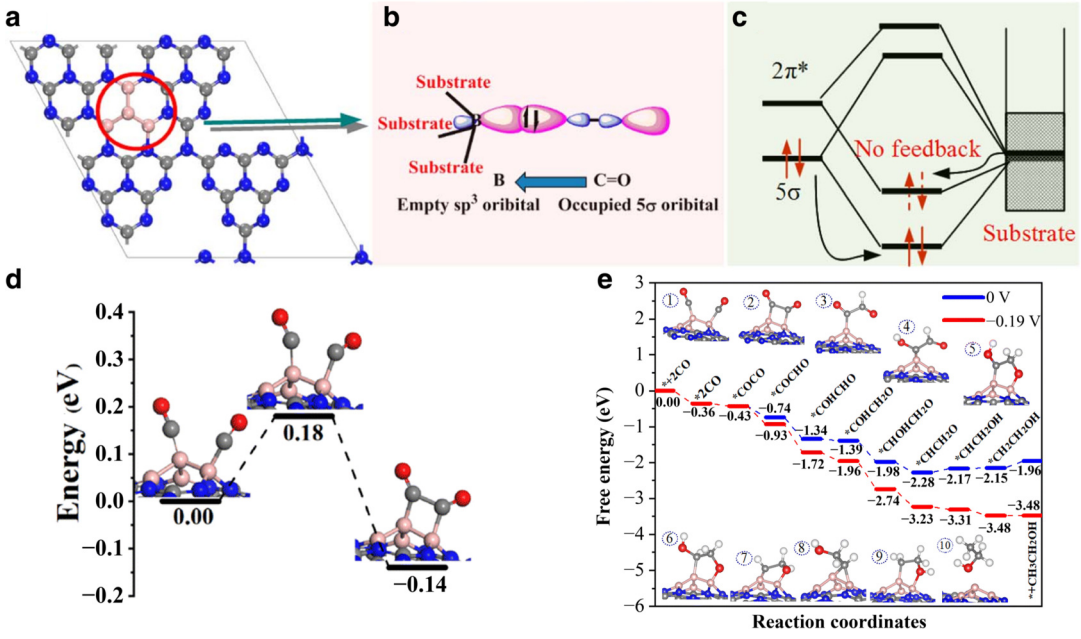

Fig. 9. The electrochemical performance of non metal MACs towards multi-carbon product. **a–c**, The structure of the tricoordinated B atom in B_4@g-C_3N_4, the bonding interactions with CO, and a simplified diagram of the orbital model. **d**, Kinetic energy barrier diagram for C–C coupling via *CO + *CO on B_4@g-C_3N_4. **e**, ΔG for CO reduction to CH_3CH_2OH on B_4@g-C_3N_4 at 0 V and −0.19 V. Reproduced with permission from Ref.[122], © Royal Society of Chemistry 2023.

endeavor, incorporating both experimental and theoretical aspects, to facilitate breakthroughs in this critical area of research.

4 Mechanism on MACs in carbon conversion

Having explored the taxonomy, synthesis routes, and detailed characterization profiles of MACs, we now focus on their critical role in the pursuit of carbon neutrality. Unlike single-atom, cluster, and nanoparticle-based catalysts, MACs stand out for their near-perfect 100% atomic efficiency combined with a strong synergistic interaction between distinct atomic sites. This dual advantage supports their exceptional potential for achieving high conversion rates at a lower cost, an important consideration for sustainable chemical processes.

The abundance of active sites in MACs highlights their effectiveness in catalyzing complex reactions involving organic molecules or larger substrates, where multiple interactions and transformations are essential. These sites, located within the architecture of MACs, enable efficient access to reactants and promote interactions, thereby enhancing overall catalytic performance. Recognizing the crucial role of MACs in advancing carbon-neutral technologies, the scientific community has actively sought to understand their underlying mechanisms. This pursuit has led to the development of numerous hypotheses, which have been rigorously examined through a multifaceted approach that includes both experimental validation and theoretical modeling. The following section will carefully summarize these insights, highlighting two key aspects.

4.1 Synergistic effect in MACs

The synergistic effect in MACs is fundamental to their remarkable catalytic performance. This effect stems from the complex interplay between diverse atomic sites, each providing distinct functionalities to the catalytic process. These sites, which often include a combination of metals, organic ligands, and potential defect structures, engage in cooperative interactions that exceed the sum of their individual contributions. Consequently, MACs can leverage complementary reaction pathways, improving both reaction rates and selectivity.

Wei and coworkers used both theoretical and experimental methods to examine the Ni and Sn pair sites[123]. As indicated by ΔG_{ads}, the NiSn pair sites present the lowest energy barrier for *OCHO formation, which facilitates CO_2 adsorption. With *COOH adsorption on Ni in NiSn-APC, the catalytic process proceeds through the lowest energy barrier of 0.53 eV (Figs. 10a and b). These findings are supported by *in situ* attenuated total reflection-infrared (ATR-IR) spectroscopy, where a band centered at 1275 cm^{-1} corresponding to $*CO_2^-$ on Ni is observed (Figs. 10c and 10d). In this system, the positively charged Sn sites help regulate the electronic structure of Ni, enhancing CO_2 adsorption. Zhang and coworkers used operando XAS to investigate the reaction intermediates[108]. XANES results (Figs. 10e–10h) reveal a slight decrease in the oxidation state at the pre-edge of dual Ni samples, attributed to charge transfer between the metal center and the reactant. Ab initio molecular dynamics simulations were also used to explore the reaction kinetics in an aqueous environment, showing that OH_{ad}-induced charge augmentation at Ni sites enhances CO_2 activation, leading to lower *COOH formation energies (Figs. 10i and 10j). Zhang and coworkers further explored the synergistic effect in heteronuclear dual-atom catalysts of Ni and Co[111]. Theoretical results indicate that the interaction between the two metal centers modulates the electronic structure, enhancing CO adsorption while simultaneously weakening hydrogen adsorption. Similarly, Pei et al. studied a comparable phenomenon in Zn–Mn dual-atom sites[114], revealing a distinct electronic structure that promotes the formation of the *COOH intermediate.

A more accurate technique, such as fs-TA spectroscopy, may be required to capture the transient intermediates during the reaction more effectively. This method is commonly used in photocatalysis

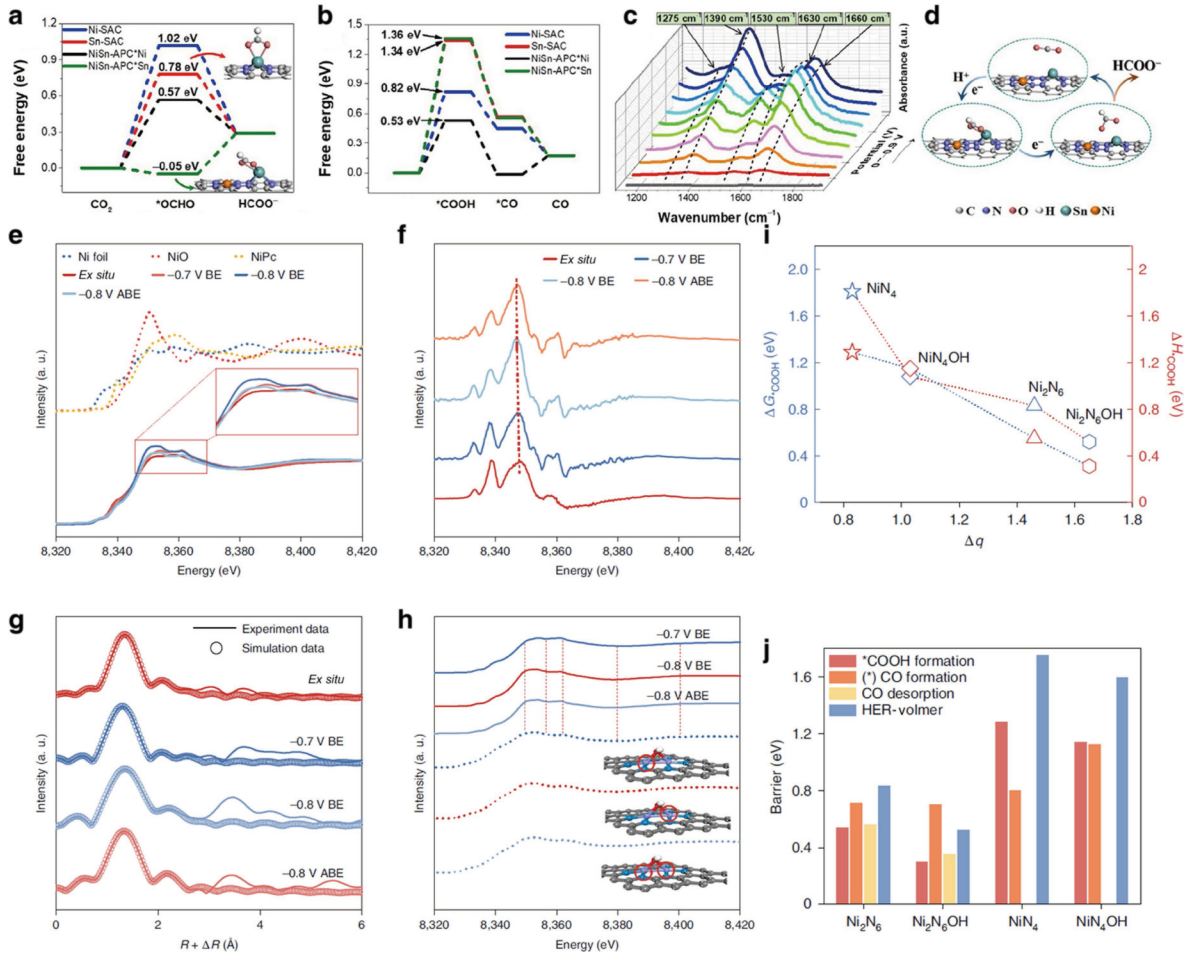

Fig. 10. The synergic effect of MACs. **a**, **b**, Free energy diagrams for CO_2RR illustrating the production of formate (a) and CO (b) on Ni-SAC, Sn-SAC, NiSn-APC*Ni, and NiSn-APC*Sn. **c**, *In situ* ATR-IR spectroscopy results for CO_2RR over NiSn-APC. **d**, A reaction pathway for CO_2RR on NiSn-APC. Reproduced with permission from Ref.[123], © Wiley-VCH GmbH 2020. **e**, XANES spectra Ni K edge for Ni_2NC at various applied potentials (V vs. RHE), with BE and ABE representing bulk electrolysis and after bulk electrolysis, respectively. **f**, The first derivative of the XANES spectra. **g**, The Fourier transform of k^3-weighted Ni K-edge EXAFS experimental and fitted data for Ni_2NC. **h**, Fitting of XANES spectra (solid lines) with the illustrated structures. The gray, turquoise, red, white, and purple spheres correspond to carbon, nitrogen, oxygen, hydrogen, and nickel atoms, respectively. **i**, The correlation between Bader charges (Δq) and Gibbs free energy/Helmholtz free energy for *COOH formation at various sites. **j**, Kinetic barriers for different adsorbates on Ni_2N_6, Ni_2N_6OH, NiN_4, and NiN_4OH sites. Reproduced with permission from Ref.[111], © Hao, Q. et al. 2022.

to detect short-lived intermediate species. Xiang's group used it to investigate the mechanism of CO_2 reduction at the dual sites of Pd and Cu (referred to as Pd_1-Cu_1/b-CN, Fig. 11)[110]. The fs-TA results revealed five dynamic decay processes at 528, 713, 745, 733, and 753 nm, which were fitted using a biexponential function (Fig. 11a). This is primarily attributed to intrinsic charge transfer (0.0798 ps, Fig. 11b), indicating that photoinduced electrons are predominantly trapped at the Pd center. The extremely fast decay time of 3.07 ps (Figs. 11c–11e) demonstrates the excellent charge transfer capability of the Cu sites, which primarily function as charge transfer conduits in the MACs system (Fig. 11f). In conclusion, the synergistic effect in the MACs considerably enhances catalytic efficiency, as demonstrated by both theoretical and experimental approaches, offering valuable insights for future MAC design.

4.2 Tandem catalytic processes on MACs

The unique structural and compositional features of MACs enable them to serve as multifunctional platforms for tandem catalytic processes. In these systems, multiple catalytic events occur in sequence in a single catalyst, eliminating the need for intermediate separation or additional catalysts. This streamlined approach simplifies workflows, reduces energy consumption, and minimizes waste. MACs' ability to host diverse active sites, each optimized for specific reaction steps, enhances their effectiveness in carrying out complex tandem reactions, thus contributing to the development of more efficient and sustainable synthetic pathways toward carbon neutrality.

The tandem effect differs from the synergistic effect because different rate-determining steps are typically carried out on various atoms in MACs. These different atoms collectively enhance efficiency during the multi-electron transfer process. Jiao et al. investigated the synergistic effect through theoretical calculations and operando attenuated total reflection surface-enhanced infrared absorption spectroscopy (ATR-SEIRAS)[113]. Adsorbed CO, used as a probe molecule for CO_2RR, exhibits a characteristic peak in the 1840–1989 cm^{-1} range (Fig. 12a). As the overpotential increases, the CO adsorption peak shifts to higher wavenumbers owing to the vibrational Stark effect. A similar phenomenon is observed at the isolated Te and Cu sites (Figs. 12b–12d). However, CO adsorption on DACs is primarily attributed to the Te SACs, suggesting that CO

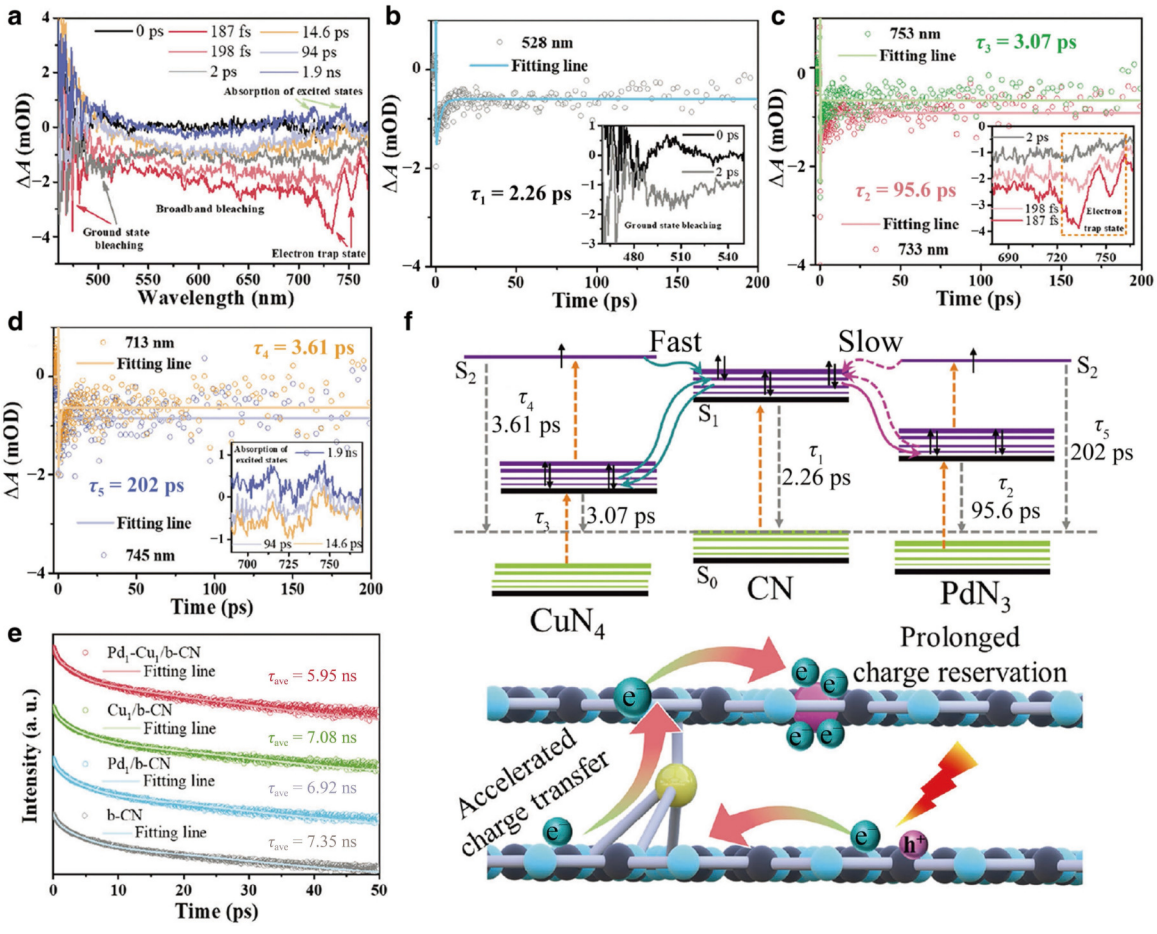

Fig. 11. The synergic effect of MACs and charge carrier kinetics analysis. **a**, fs-TA spectra of Pd_1-Cu_1/b-CN at various probe delays under 365 nm excitation. **b–d**, TA kinetic traces probed at (b) 528 nm, (c) 733 and 753 nm, and (d) 713 and 745 nm for Pd_1-Cu_1/b-CN. **e**, time-resolved transient PL decay. **f**, Schematic of dynamic charge transfer on Pd_1-Cu_1/b-CN during photocatalysis, illustrating cascade functions across interplanar and in-plane dual single atoms in layer-stacked bulk-like g-C_3N_4. Reproduced with permission from Ref.[110], © Wiley-VCH GmbH 2023.

molecules preferentially adsorb on Te. Additionally, a broad peak ranging from 3450 to 3480 cm^{-1} indicates that water molecules tend to adsorb on the Cu sites (Figs. 12e and 12f). Thus, it can be concluded that the Te center activates CO_2, while the Cu center facilitates H_2O dissociation, generating the necessary protons and enhancing efficiency through a tandem mechanism. Hou's group performed calculations and operando IR studies based on the MACs of In and Ni atomic sites (Fig. 12g)[107]. The Gibbs free energy calculations indicate that the formation of *COOH occurs first on Ni, followed by subsequent steps on In. The heteroatom system accelerates both steps, resulting in high efficiency in CO production (Figs. 12h and 12i).

By analyzing these two fundamental mechanisms, we gain a deeper understanding of the transformative potential of MACs in catalysis and their essential role in the global pursuit of carbon neutrality. The results indicate that while the mechanism is recognized as important, it has not been sufficiently studied, primarily owing to limitations in operando techniques. This underscores the need for more accurate and rapid characterization methods to directly capture the rapidly disappearing active intermediates. Combining these approaches with EPR could enhance our exploration of the radical properties of MACs, further elucidating their mechanisms.

5 Challenges

In the field of chemical engineering and catalysis, MACs face numerous challenges in the context of CO_2RR despite their remarkable potential. The strong stability of the carbon–oxygen double bond (C=O) in CO_2 requires that researchers develop highly active and selectively tailored catalysts. This endeavor is crucial because it determines the efficiency and feasibility of transforming CO_2, a greenhouse gas, into valuable chemical feedstocks.

The complexity of the reduction process, which often results in a mixture of chemical species, presents considerable challenges in product segregation and purification[124–128]. This complex product distribution requires the development of advanced separation technologies to effectively isolate and purify the desired products, thereby improving overall process economics and sustainability[129–132].

Furthermore, the longevity and stability of MACs under prolonged exposure to electrochemical conditions present considerable challenges that require substantial attention and innovative solutions. These conditions, often marked by high temperatures, corrosive electrolytes, and continuous potential fluctuations, can result in structural degradation, compositional changes, or even complete catalyst deactivation, thereby reducing their effectiveness[133–137]. Ensuring the durability of MACs under

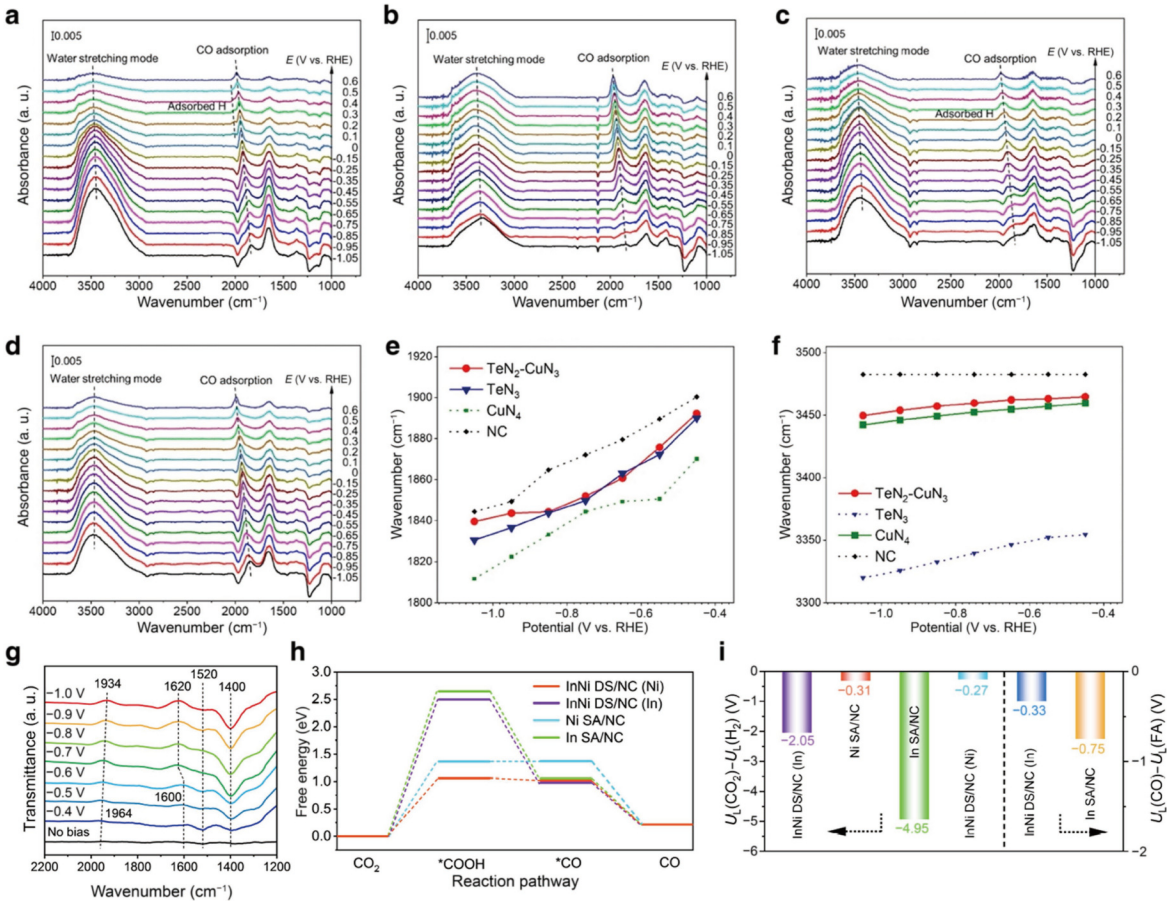

Fig. 12. The tandem catalytic process of MACs. a–d, Spectral profiles of TeN_2-CuN_3 (a), TeN_3 (b), CuN_4 (c), and CN (d) catalysts in CO_2-saturated $KHCO_3$ solution. **e**, **f**, Plots showing potential versus wavenumbers for CO adsorption (e) and water stretching modes (f) in ATR-SEIRAS spectra. Reproduced with permission from Ref.[113], © Jiao, J. et al. 2023. **g**, *In situ* ATR-SEIRAS spectra of InNi DS/NC. **h**, Calculated free energy diagrams for electrocatalytic CO_2 to CO. **i**, the $UL_{(CO_2)}$, $UL_{(H_2)}$ and $UL_{(CO)}$, $UL_{(FA)}$ values of In and Ni sites in different catalysts. Reproduced with permission from Ref.[106], © Wiley-VCH GmbH 2022.

operational settings is crucial for maintaining consistent catalytic performance over extended periods. This requires not only robust design strategies capable of withstanding the harsh electrochemical environment but also a comprehensive understanding of the underlying degradation mechanisms. Researchers must explore the complex interplay between catalyst structure, surface chemistry, and the surrounding reaction medium to develop strategies for mitigating adverse effects and extending catalyst lifespan. Additionally, scaling up the production of MACs to meet industrial demands presents another considerable challenge. The synthesis protocols typically involve complex, multistep processes that are difficult to reproduce consistently at large scales, impacting both yield and quality. Cost-effectiveness in manufacturing is also critical for industrial adoption, requiring optimization efforts to minimize raw material consumption, energy use, and waste generation.

To address these challenges, researchers are adopting a multifaceted approach, using the latest advancements in materials science and catalysis. Firstly, there is a concerted effort aimed at the precise synthesis of MACs, focusing on the rational design of metal-support interfaces to optimize interactions and enhance catalytic activity and selectivity. This includes exploring novel support materials and fine-tuning metal loading and dispersion.

Secondly, the integration of promoters or additives into SAC systems is being actively explored as a means to further enhance catalytic performance. These additives can function as electron modifiers (adjusting the electronic structure of the active sites) or as structural promoters (improving the stability and accessibility of the catalytic sites).

Additionally, developing advanced reactor systems designed for efficient product separation and recycling is crucial. Such systems aim to minimize product loss during separation, enhance energy efficiency, and facilitate the recycling of unreacted reactants and intermediates, thereby improving overall process sustainability.

Lastly, the synergy between computational modeling and machine learning techniques is transforming the field. These tools facilitate the prediction and optimization of MACs' properties and performance in CO_2RR, considerably accelerating the discovery and development of novel catalysts. By simulating and predicting catalytic behavior at the atomic scale, researchers can identify promising candidates and direct experimental efforts toward targeted improvements.

In conclusion, addressing the challenges faced by MACs in CO_2RR applications requires a comprehensive approach that includes advancements in synthesis, characterization, reactor design, and computational modeling. This concerted effort promises to unlock the full potential of MACs, paving the way for the large-scale use of CO_2 as a sustainable chemical feedstock.

References

[1] Qiao, B. T.; Wang, A. Q.; Yang, X. F.; Allard, L. F.; Jiang, Z.; Cui, Y. T.; Liu, J. Y.; Li, J.; Zhang, T. Single-atom catalysis of CO oxidation using Pt_1/FeO_x. *Nat. Chem.* **2011**, *3*, 634–641.

[2] Tang, T. M.; Wang, Z. L.; Guan, J. Q. Structural optimization of carbon-based diatomic catalysts towards advanced electrocatalysis. *Coord. Chem. Rev.* **2023**, *492*, 215288.

[3] Zha, W.; Liu, D. W.; Ma, Z. J.; Wang, Y. Z.; Wei, Y. O. N. C.; Ma, X. F. N.; Wang, L. L.; Zhang, Q. Q.; Lou, B. Y.; Yuan, R. S. et al. Efficient electrochemical CO_2 reduction on C_2N monolayer supported transition metals trimer catalysts: A DFT study. *Appl. Surf. Sci.* **2021**, *564*, 150331.

[4] Yang, X. F.; Wang, A.; Qiao, B. T.; Li, J.; Liu, J. Y.; Zhang, T. Single-atom catalysts: A new frontier in heterogeneous catalysis. *Acc. Chem. Res.* **2013**, *46*, 1740–1748.

[5] Gloag, L.; Somerville, S. V.; Gooding, J. J.; Tilley, R. D. Co-catalytic metal-support interactions in single-atom electrocatalysts. *Nat. Rev. Mater.* **2024**, *9*, 173–189.

[6] Zeng, L.; Cheng, K.; Sun, F. F.; Fan, Q. Y.; Li, L. Y.; Zhang, Q. H.; Wei, Y.; Zhou, W.; Kang, J. C.; Zhang, Q. Y. et al. Stable anchoring of single rhodium atoms by indium in zeolite alkane dehydrogenation catalysts. *Science* **2024**, *383*, 998–1004.

[7] Hai, X.; Zheng, Y.; Yu, Q.; Guo, N.; Xi, S. B.; Zhao, X. X.; Mitchell, S.; Luo, X. H.; Tulus, V.; Wang, M. et al. Geminal-atom catalysis for cross-coupling. *Nature* **2023**, *622*, 754–760.

[8] Shi, Z. Y.; Zhang, X.; Lin, X. Q.; Liu, G. G.; Ling, C. Y.; Xi, S. B.; Chen, B.; Ge, Y. Y.; Tan, C. L.; Lai, Z. C. et al. Phase-dependent growth of Pt on MoS_2 for highly efficient H_2 evolution. *Nature* **2023**, *621*, 300–305.

[9] Gu, J.; Jian, M. Z.; Huang, L.; Sun, Z. H.; Li, A. W.; Pan, Y.; Yang, J. Z.; Wen, W.; Zhou, W.; Lin, Y. et al. Synergizing metal-support interactions and spatial confinement boosts dynamics of atomic nickel for hydrogenations. *Nat. Nanotechnol.* **2021**, *16*, 1141–1149.

[10] Yang, J. R.; Li, W. H.; Wang, D. S.; Li, Y. D. Electronic metal-support interaction of single-atom catalysts and applications in electrocatalysis. *Adv. Mater.* **2020**, *32*, 2003300.

[11] Zhu, E. Z.; Zheng, T. L.; Yu, J.; Shi, C. Y.; Zhou, L. X.; Jin, H. D.; Yang, J. R.; Luo, G. T.; Wei, D. Y.; Yang, X. K. et al. Electron redistribution and proton transfer induced by atomically fully exposed Cu–O–Fe clusters coupled with single-atom sites for efficient oxygen electrocatalysis. *Energy Storage Mater.* **2024**, *69*, 103410.

[12] Yang, J. R.; Li, W. H.; Wang, D. S.; Li, Y. D. Single-atom materials: Small structures determine macroproperties. *Small Struct.* **2021**, *2*, 2000051.

[13] Yang, L.; Feng, S. H.; Zhu, W. H. Achieving reaction pathway separation for electrochemical nitrate fixation on triatomic catalysts: A new mechanism. *J. Hazard. Mater.* **2023**, *441*, 129972.

[14] Chen, Z. Y.; Su, X. Z.; Ding, J.; Yang, N.; Zuo, W. B.; He, Q. Y.; Wei, Z. M.; Zhang, Q.; Huang, J.; Zhai, Y. M. Boosting oxygen reduction reaction with Fe and Se dual-atom sites supported by nitrogen-doped porous carbon. *Appl. Catal. B: Environ.* **2022**, *308*, 121206.

[15] Yang, J. R.; Li, W. H.; Tan, S. D.; Xu, K. N.; Wang, Y.; Wang, D. S.; Li, Y. D. The electronic metal-support interaction directing the design of single atomic site catalysts: Achieving high efficiency towards hydrogen evolution. *Angew. Chem.* **2021**, *133*, 19233–19239.

[16] Wang, L. W.; Liu, P. F.; Yang, J.; Liang, C. J.; Deng, C. S.; Zhao, Y. X.; Guo, X. F.; Peng, L. M.; Xue, N. H.; Wang, Q. CO_2 electroreduction to acetate by enhanced tandem effects of surface intermediate over Co_3O_4 supported polyaniline catalyst. *Carbon Future* **2024**, *1*, 9200013.

[17] Li, W. H.; Yang, J. R.; Wang, D. S. Long-range interactions in diatomic catalysts boosting electrocatalysis. *Angew. Chem.* **2022**, *134*, e202213318.

[18] Song, X. Y.; Diao, S. Y.; He, W. J.; Yang, J.; Wang, L. L.; Qin, G.; Li, Y.; Chen, Q. Design of active dual atom Ni–Co–2H–MoS_2 catalyst: Synergistic effect of Ni-adsorption and co-catalysis for activating peroxymonosulfate. *Sep. Purif. Technol.* **2024**, *333*, 125927.

[19] Wang, X. Y.; Pan, Y. Z.; Yang, J. R.; Li, W. H.; Gan, T.; Pan, Y. M.; Tang, H. T.; Wang, D. S. Single-atom iron catalyst as an advanced redox mediator for anodic oxidation of organic electrosynthesis. *Angew. Chem., Int. Ed.* **2024**, *63*, e202404295.

[20] Zhao, J.; Zhang, Y. X.; Zhuang, Z. C.; Deng, Y. T.; Gao, G.; Li, J. Y.; Meng, A. L.; Li, G. C.; Wang, L.; Li, Z. J. et al. Tailoring d-p orbital hybridization to decipher the essential effects of heteroatom substitution on redox kinetics. *Angew. Chem.* **2024**, *136*, e202404968.

[21] Zhang, Y. D.; Sun, Y. J.; Wang, Q. Y.; Zhuang, Z. C.; Ma, Z. T.; Liu, L. M.; Wang, G. M.; Wang, D. S.; Zheng, X. S. Synergy of photogenerated electrons and holes toward efficient photocatalytic urea synthesis from CO_2 and N_2. *Angew. Chem., Int. Ed.* **2024**, *63*, e202405637.

[22] Mu, X. Q.; Liu, S. L.; Zhang, M. Y.; Zhuang, Z. C.; Chen, D.; Liao, Y. R.; Zhao, H. Y.; Mu, S. C.; Wang, D. S.; Dai, Z. H. Symmetry-broken Ru nanoparticles with parasitic Ru–Co dual-single atoms overcome the volmer step of alkaline hydrogen oxidation. *Angew. Chem.* **2024**, *136*, e202319618.

[23] Qiu, W. B.; Qin, S. M.; Li, Y. B.; Cao, N.; Cui, W. R.; Zhang, Z. D.; Zhuang, Z. C.; Wang, D. S.; Zhang, Y. Overcoming electrostatic interaction via pulsed electroreduction for boosting the electrocatalytic urea synthesis. *Angew. Chem.* **2024**, *136*, e202402684.

[24] Liu, Y. L.; Zhuang, Z. C.; Liu, Y. X.; Liu, N. Y.; Li, Y. X.; Cheng, Y. Y.; Yu, J. W.; Yu, R. H.; Wang, D. S.; Li, H. T. Shear-strained Pd single-atom electrocatalysts for nitrate reduction to ammonia. *Angew. Chem., Int. Ed.*, in press, DOI: 10.1002/anie.202411396.

[25] Zhang, Z. D.; Zhu, J. X.; Chen, S. H.; Sun, W. M.; Wang, D. S. Liquid fluxional Ga single atom catalysts for efficient electrochemical CO_2 reduction. *Angew. Chem.* **2023**, *135*, e202215136.

[26] Tang, H. T.; Zhou, H. Y.; Pan, Y. M.; Zhang, J. L.; Cui, F. H.; Li, W. H.; Wang, D. S. Single-atom manganese-catalyzed oxygen evolution drives the electrochemical oxidation of silane to silanol. *Angew. Chem.* **2024**, *136*, e202315032.

[27] Chen, S. H.; Ye, C. L.; Wang, Z. W.; Li, P.; Jiang, W. J.; Zhuang, Z. C.; Zhu, J. X.; Zheng, X. B.; Zaman, S.; Ou, H. H. Selective CO_2 reduction to ethylene mediated by adaptive small-molecule engineering of copper-based electrocatalysts. *Angew. Chem.* **2023**, *135*, e202315621.

[28] Ning, S. B.; Ou, H. H.; Li, Y. G.; Lv, C. C.; Wang, S. F.; Wang, D. S.; Ye, J. H. Co^0–$Co^{\delta+}$ interface double-site-mediated C–C coupling for the photothermal conversion of CO_2 into light olefins. *Angew. Chem., Int. Ed.* **2023**, *62*, e202302253.

[29] Hu, Y. M.; Chao, T. T.; Li, Y. P.; Liu, P. G.; Zhao, T. H.; Yu, G.; Chen, C.; Liang, X.; Jin, H. L.; Niu, S. W. et al. Cooperative Ni(Co)–Ru–P sites activate dehydrogenation for hydrazine oxidation assisting self-powered H_2 production. *Angew. Chem.* **2023**, *135*, e202308800.

[30] Gao, Y.; Wang, D. S. Atomically dispersed catalysts: Precise synthesis, structural regulation, and structure-activity relationship. *CCS Chem.* **2024**, *6*, 833–855.

[31] Zhou, A. W.; Wang, D. S.; Li, Y. D. Hollow microstructural regulation of single-atom catalysts for optimized electrocatalytic performance. *Microstructures* **2022**, *2*, 2022005.

[32] Gan, T.; Wang, D. S. Atomically dispersed materials: Ideal catalysts in atomic era. *Nano Res.* **2024**, *17*, 18–38.

[33] Wang, L. G.; Wu, J. B.; Wang, S. W.; Liu, H.; Wang, Y.; Wang, D. S. The reformation of catalyst: From a trial-and-error synthesis to rational design. *Nano Res.* **2024**, *17*, 3261–3301.

[34] Zhuang, J. H.; Wang, D. S. Recent advances of single-atom alloy catalyst: Properties, synthetic methods and electrocatalytic applications. *Mater. Today Catal.* **2023**, *2*, 100009.

[35] Wang, Y.; Zheng, X. B.; Wang, D. S. Design concept for electrocatalysts. *Nano Res.* **2022**, *15*, 1730–1752.

[36] Li, R. Z.; Wang, D. S. Understanding the structure-performance relationship of active sites at atomic scale. *Nano Res.* **2022**, *15*, 6888–6923.

[37] Zheng, X. B.; Li, B. B.; Wang, Q. S.; Wang, D. S.; Li, Y. D. Emerging low-nuclearity supported metal catalysts with atomic level precision for efficient heterogeneous catalysis. *Nano Res.* **2022**, *15*,

7806–7839.
[38] Wang, L. G.; Wang, D. S.; Li, Y. D. Single-atom catalysis for carbon neutrality. *Carbon Energy* **2022**, *4*, 1021–1079.
[39] Wu, Y.; Tan, S. J.; Zhang, T. C.; Zhou, M.; Fang, G.; Ji, G. B. Alkali and ion exchange co-modulation strategies to design magnetic-dielectric synergistic nano-absorbers for tailoring microwave absorption. *Nano Res.* **2023**, *16*, 8522–8532.
[40] Zhang, C. M.; Liang, L.; Zhao, S. L.; Wu, Z. J.; Wang, S. H.; Yin, D. M.; Wang, Q. S.; Wang, L. M.; Wang, C. L.; Cheng, Y. Dehydrogenation behavior and mechanism of $LiAlH_4$ adding nano-CeO_2 with different morphologies. *Nano Res.* **2023**, *16*, 9426–9434.
[41] Chopra, D.; Guo, T. Q.; Ivanovski, S.; Gulati, K. Single-step nano-engineering of multiple micro-rough metals via anodization. *Nano Res.* **2023**, *16*, 1320–1329.
[42] Han, Y. X.; He, M. K.; Hu, J. W.; Liu, P. B.; Liu, Z. W.; Ma, Z. L.; Ju, W. B.; Gu, J. W. Hierarchical design of FeCo-based microchains for enhanced microwave absorption in C band. *Nano Res.* **2023**, *16*, 1773–1778.
[43] Gao, Y. Z.; Zhang, W. Y.; Choi, C.; Shang, B.; Cheon, S.; Meese, A. F.; Kim, J. H.; Long, D. H.; Fortner, J.; Wang, H. L. Effective electrochemical trichloroethylene removal from water enabled by selective molecular catalysis. *Carbon Future* **2024**, *1*, 9200015.
[44] Wang, W. H.; Wang, Y.; Kong, X. J.; Ning, H.; Wu, M. B. Carbon-based material for CO_2 catalytic conversion applications. *Carbon Future* **2024**, *1*, 9200016.
[45] Hou, Z. L.; Du, K. R.; Zhang, Y. Q.; Bi, S.; Zhang, J. Y. Nanoarchitectonics of MnO_2 nanotubes as sea urchin-like aggregates for dielectric response and microwave absorption with a wide concentration domain. *Nano Res.* **2023**, *16*, 2604–2610.
[46] Wang, B. J.; Huang, F. Z.; Wu, H.; Xu, Z. J.; Wang, S. P.; Han, Q. H.; Liu, F. H.; Li, S. K.; Zhang, H. Enhanced interfacial polarization of defective porous carbon confined CoP nanoparticles forming Mott-Schottky heterojunction for efficient electromagnetic wave absorption. *Nano Res.* **2023**, *16*, 4160–4169.
[47] Feng, Y. D.; Tu, C.; Li, R. J.; Wu, D.; Yang, J.; Xia, Y. K.; Peijnenburg, W. J. G. M.; Luo, Y. M. A systematic review of the impacts of exposure to micro-and nano-plastics on human tissue accumulation and health. *Eco-Environ. Health* **2023**, *2*, 195-207.
[48] Ouyang, B.; Qin, H. N.; Sun, C.; Deng, Y. L.; Li, A.; Zhu, J. P.; Kan, E. J.; Rawat, R. S. Tailored heterostructured Ni_3N–NiO nano-frameworks for boosting electrocatalytic oxygen evolution via surface-modulated plasma strategy. *Nano Res.* **2024**, *17*, 7909–7917.
[49] Li, Z. S.; Li, B. L.; Yu, M.; Yu, C. L.; Shen, P. K. Amorphous metallic ultrathin nanostructures: A latent ultra-high-density atomic-level catalyst for electrochemical energy conversion. *Int. J. Hydrogen Energy* **2022**, *47*, 26956–26977.
[50] Dai, X. Y.; Yan, P. Q.; Bai, Y. L.; Guo, M.; Qi, W. Phosphorus modified onion-like carbon catalyzed methanol conversion to dimethoxymethane: The unique role of P–C species. *Carbon Future* **2024**, *1*, 9200012.
[51] Cao, G. B.; Xing, H. R.; Gui, H. G.; Yao, C.; Chen, Y. J.; Chen, Y. S.; Li, X. Z. Plasmonic quantum dots modulated nano-mineral toward photothermal reduction of CO_2 coupled with biomass conversion. *Nano Res.* **2024**, *17*, 5061–5072.
[52] Xu, H. X.; He, Z. Z.; Wang, Y. R.; Ren, X. R.; Liu, P. B. Metal-phenolic coordination crystals derived magnetic hollow carbon spheres for ultrahigh electromagnetic wave absorption. *Nano Res.* **2024**, *17*, 1616–1624.
[53] Yang, J. R.; Li, W. H.; Xu, K. N.; Tan, S. D.; Wang, D. S.; Li, Y. D. Regulating the tip effect on single-atom and cluster catalysts: Forming reversible oxygen species with high efficiency in chlorine evolution reaction. *Angew. Chem.* **2022**, *134*, e202200366.
[54] Xue, Z.; Yu, W. W.; Zhang, T.; He, S. Y.; Zhao, W. T.; Wang, B. J.; Liu, Y. F.; Zou, B. X.; Zhang, R. G.; Zhao, Z. K. Adjacent diatomic Cu_1N_3/Mo_1S_2 entities decorated carbon nitride for markedly enhanced photocatalytic hydrogen generation. *Chem. Eng. J.* **2023**, *463*, 142470.
[55] Kuhn, A. N.; Park, R. C.; Yu, S. Y.; Gao, D.; Zhang, C.; Zhang, Y. H.; Yang, H. Valorization of carbon dioxide into C1 product via reverse water gas shift reaction using oxide-supported molybdenum carbides. *Carbon Future* **2024**, *1*, 9200011.
[56] Zhu, H. J.; Li, M. H.; Zou, L. N.; Hu, Y. Y.; Hao, H. G.; Dou, J. M.; Mao, J. J. A study on singlet oxygen generation for tetracycline degradation via modulating the size of α-Fe_2O_3 nanoparticle anchored on g-C_3N_4 nanotube photocatalyst. *Nano Res.* **2023**, *16*, 2236–2244.
[57] Yang, J. R.; Li, W. H.; Tang, H. T.; Pan, Y. M.; Wang, D. S.; Li, Y. D. CO_2-mediated organocatalytic chlorine evolution under industrial conditions. *Nature* **2023**, *617*, 519–523.
[58] Zhang, L. L.; Shi, X. X.; Xu, A. J.; Zhong, W. W.; Zhang, J. T.; Shen, S. J. Novel CoP/$CoMoP_2$ heterojunction with nanoporous structure as an efficient electrocatalyst for hydrogen evolution. *Nano Res.* **2024**, *17*, 3693–3699.
[59] Li, R. S.; Gu, C. S.; Rao, P.; Deng, P. L.; Wu, D. X.; Luo, J. M.; Li, J.; Miao, Z. P.; Zheng, C. W.; Shen, C. et al. Ternary single atom catalysts for effective oxygen reduction and evolution reactions. *Chem. Eng. J.* **2023**, *468*, 143641.
[60] Zhu, C. X.; Yang, J. R.; Zhang, J. W.; Wang, X. Q.; Gao, Y.; Wang, D. S.; Pan, H. G. Single-atom materials: The application in energy conversion. *Interdiscip. Mater.* **2024**, *3*, 74–86.
[61] Jiang, B.; Guo, Z. J.; Liang, M. M. Recent progress in single-atom nanozymes research. *Nano Res.* **2023**, *16*, 1878–1889.
[62] Wu, J. G.; Li, X.; Fu, K.; Cao, D.; Cheng, D. J. Constructing fully exposed Pt atomically dispersed catalysts for enhanced multifunctional selective hydrogenation reactions. *Chem. Eng. J.* **2024**, *481*, 148706.
[63] Shukla, S.; Pei, Y.; Li, W. G.; Pei, D. S. Toxicological research on Nano and microplastics in environmental pollution: Current advances and future directions. *Aquat. Toxicol.* **2024**, *270*, 106894.
[64] Mitrano, D. M.; Diamond, M. L.; Kim, J. H.; Tam, K. C.; Yang, M.; Wang, Z. Y. Balancing new approaches and harmonized techniques in nano-and microplastics research. *ACS Sustain. Chem. Eng.* **2023**, *11*, 8702–8705.
[65] Yang, J. R.; Zhu, C. X.; Li, W. H.; Zheng, X. S.; Wang, D. S. Organocatalyst supported by a single-atom support accelerates both electrodes used in the chlor-alkali industry via modification of non-covalent interactions. *Angew. Chem., Int. Ed.* **2024**, *63*, e202314382.
[66] Hao, Q.; Tang, Q.; Zhong, H. X.; Wang, J. Z.; Liu, D. X.; Zhang, X. B. Fully exposed nickel clusters with electron-rich centers for high-performance electrocatalytic CO_2 reduction to CO. *Sci. Bull.* **2022**, *67*, 1477–1485.
[67] Yang, J. R.; Wang, D. S.; Li, Y. D. Identifying the types and characterization of the active sites on M−X−C single-atom catalysts. *ChemPhysChem* **2020**, *21*, 2486–2496.
[68] Zheng, T. T.; Jiang, K.; Ta, N.; Hu, Y. F.; Zeng, J.; Liu, J. Y.; Wang, H. T. Large-scale and highly selective CO_2 electrocatalytic reduction on nickel single-atom catalyst. *Joule* **2019**, *3*, 265–278.
[69] Zhang, Y. F.; Li, Z. W.; Zhang, J. J.; Xu, L. L.; Han, Z. K.; Baiker, A.; Li, G. Nanostructured Ni-MoC_x: An efficient non-noble metal catalyst for the chemoselective hydrogenation of nitroaromatics. *Nano Res.* **2023**, *16*, 8919–8928.
[70] Zhang, Z. J.; Liu, Y.; Su, X. Z.; Zhao, Z. W.; Mo, Z. K.; Wang, C. Y.; Zhao, Y. L.; Chen, Y.; Gao, S. Y. Electro-triggered Joule heating method to synthesize single-phase CuNi nano-alloy catalyst for efficient electrocatalytic nitrate reduction toward ammonia. *Nano Res.* **2023**, *16*, 6632–6641.
[71] Sun, H. N.; Xu, X. M.; Chen, G.; Shao, Z. P. Perovskite oxides as electrocatalysts for water electrolysis: From crystalline to amorphous. *Carbon Energy*, in press, DOI: 10.1002/cey2.595.
[72] Peng, J. Z.; Li, Y. L.; Cheng, Y. T.; Li, F. Z.; Cao, B.; Wang, Q.; Yue, X.; Lai, G. T.; Wang, Y. G.; Gu, J. Metal-N_4 model single-atom catalyst with electroneutral quadri-pyridine macrocyclic ligand for CO_2 electroreduction. *Carbon Energy* **2024**, *6*, e506.
[73] Yuan, Y. P.; Zheng, Y.; Luo, D.; Qiu, W. B.; Wang, J. T.; Wang, X.; Chen, Z. W. Recent progress on mechanisms, principles, and strategies for high-activity and high-stability non-PGM fuel cell catalyst design. *Carbon Energy* **2024**, *6*, e426.
[74] Yang, J. R.; Li, W. H.; Wang, D. S. Machine learning: The trends of developing high-efficiency single-atom materials. *Chem Catal.* **2021**, *1*, 24–26.
[75] Li, L. F.; Zhu, J. M.; Kong, F. P.; Wang, Y. J.; Kang, C.; Xu, M.; Du, C. Y.; Yin, G. P. Tailoring atomic strain environment for high-performance acidic oxygen reduction by Fe–Ru dual atoms communicative effect. *Matter* **2024**, *7*, 1517–1532.

[76] Yang, J. R.; Zhu, C. X.; Yang, C. J.; Li, W. H.; Zhou, H. Y.; Tan, S. D.; Liu, X. W.; He, D. P.; Wang, D. S. Accelerating the hydrogen production via modifying the Fermi surface. *Nano Lett.* **2023**, *23*, 11368–11375.

[77] Chougule, S. S.; Jeffery, A. A.; Roy Chowdhury, S.; Min, J.; Kim, Y.; Ko, K.; Sravani, B.; Jung, N. Antipoisoning catalysts for the selective oxygen reduction reaction at the interface between metal nanoparticles and the electrolyte. *Carbon Energy* **2023**, *5*, e293.

[78] Zhang, B. X.; Chen, Y. P.; Wang, J. M.; Pan, H. G.; Sun, W. P. Supported sub-nanometer clusters for electrocatalysis applications. *Adv. Funct. Mater.* **2022**, *32*, 2202227.

[79] Gandionco, K. A.; Kim, J.; Bekaert, L.; Hubin, A.; Lim, J. Single-atom catalysts for the electrochemical reduction of carbon dioxide into hydrocarbons and oxygenates. *Carbon Energy* **2024**, *6*, e410.

[80] Guo, B. W.; Wang, Z. K.; Zheng, L.; Mo, G.; Zhou, H. J.; Luo, D. Confined cobalt single-atom catalysts with strong electronic metal-support interactions based on a biomimetic self-assembly strategy. *Carbon Energy*, in press, DOI: 10.1002/cey2.554.

[81] Yang, J. R.; Zhu, C. X.; Wang, D. S. A simple organo-electrocatalysis system for the chlor-related industry. *Angew. Chem., Int. Ed.* **2024**, *63*, e202406883.

[82] Hossain, M. D.; Liu, Z. J.; Zhuang, M. H.; Yan, X. X.; Xu, G. L.; Gadre, C. A.; Tyagi, A.; Abidi, I. H.; Sun, C. J.; Wong, H. et al. Rational design of graphene-supported single atom catalysts for hydrogen evolution reaction. *Adv. Energy Mater.* **2019**, *9*, 1803689.

[83] Yang, J. R.; Pei, J. J.; Dong, J. C.; Wang, D. S. Accurate synthesis and industrial production of single-atom catalysts. *Chem Catal.* **2022**, *2*, 2111–2113.

[84] Chang, F. F.; Zhang, Z. M.; Zhang, Y.; Liu, Y. P.; Yang, L.; Wang, X. L.; Bai, Z. Y.; Zhang, Q. Synergistic modulation of valence state and oxygen vacancy induced by surface reconstruction of the CeO_2/CuO catalyst toward enhanced electrochemical CO_2 reduction. *Carbon Energy*, in press, DOI: 10.1002/cey2.588.

[85] Song, Z. X.; Li, J. J.; Zhang, Q. L.; Li, Y. L.; Ren, X. Z.; Zhang, L.; Sun, X. L. Progress and perspective of single-atom catalysts for membrane electrode assembly of fuel cells. *Carbon Energy* **2023**, *5*, e342.

[86] Hwang, C. K.; Kim, S.; Yoon, K. R.; Le, T. T.; Hoang, C. V.; Choi, J. W.; Zhang, W. J.; Paek, S. Y.; Lee, C. H.; Lee, J. H. et al. Arc plasma-deposited Co single-atom catalysts supported on an aligned carbon nanofiber for hydrogen peroxide electrosynthesis and an electro-Fenton process. *Carbon Energy*, in press, DOI: 10.1002/cey2.582.

[87] Li, R. Z.; Wang, D. S. Superiority of dual-atom catalysts in electrocatalysis: One step further than single-atom catalysts. *Adv. Energy Mater.* **2022**, *12*, 2103564.

[88] Yang, X. X.; Liang, J. S.; Shi, Q. R.; Zachman, M. J.; Kabir, S.; Liang, J. W.; Zhu, J.; Slenker, B.; Pupucevski, M.; Macauley, N. et al. Regulating the third metal to design and engineer multilayered NiFeM (M: Co, Mn, and Cu) nanofoam anode catalysts for anion-exchange membrane water electrolyzers. *Adv. Energy Mater.* **2024**, *14*, 2400029.

[89] Chen, Y.; Lin, J.; Jia, B. H.; Wang, X. D.; Jiang, S. Y.; Ma, T. Y. Isolating single and few atoms for enhanced catalysis. *Adv. Mater.* **2022**, *34*, 2201796.

[90] Gao, Y.; Liu, B. Z.; Wang, D. S. Microenvironment engineering of single/dual-atom catalysts for electrocatalytic application. *Adv. Mater.* **2023**, *35*, 2209654.

[91] Zhu, Y. P.; Fan, K.; Hsu, C. S.; Chen, G.; Chen, C. S.; Liu, T. C.; Lin, Z. Z.; She, S. X.; Li, L. Q.; Zhou, H. M. et al. Supported ruthenium single-atom and clustered catalysts outperform benchmark Pt for alkaline hydrogen evolution. *Adv. Mater.* **2023**, *35*, 2301133.

[92] Wang, J. Y.; Shao, Y. Y.; Zhu, J. Improving flow and fluidization quality of fine and ultrafine particles via nanoparticle modulation. *Nano Res.* **2023**, *16*, 12013–12025.

[93] Sun, Z. Y.; Li, C.; Wei, Z. H.; Zhang, F.; Deng, Z. W.; Zhou, K. J.; Wang, Y.; Guo, J. H.; Yang, J. Y.; Xiang, Z. Q. et al. Sulfur-bridged asymmetric CuNi bimetallic atom sites for CO_2 reduction with high efficiency. *Adv. Mater.* **2024**, *36*, 2404665.

[94] Duan, J. J.; Chen, S.; Ortíz-Ledón, C. A.; Jaroniec, M.; Qiao, S. Z. Phosphorus vacancies that boost electrocatalytic hydrogen evolution by two orders of magnitude. *Angew. Chem.* **2020**, *132*, 8258–8263.

[95] Pan, L.; Wang, J. N.; Lu, F.; Liu, Q.; Gao, Y. H.; Wang, Y.; Jiang, J. Z.; Sun, C.; Wang, J.; Wang, X. Single-atom or dual-atom in TiO_2 nanosheet: Which is the better choice for electrocatalytic urea synthesis. *Angew. Chem.* **2023**, *135*, e202216835.

[96] Pei, Z. H.; Lu, X. F.; Zhang, H. B.; Li, Y. X.; Luan, D. Y.; Lou, X. W. Highly efficient electrocatalytic oxygen evolution over atomically dispersed synergistic Ni/Co dual sites. *Angew. Chem.* **2022**, *134*, e202207537.

[97] Duan, L. L.; Hung, C. T.; Wang, J. X.; Wang, C. Y.; Ma, B.; Zhang, W.; Ma, Y. Z.; Zhao, Z. W.; Yang, C. C.; Zhao, T. C. et al. Synthesis of fully exposed single-atom-layer metal clusters on 2D ordered mesoporous TiO_2 nanosheets. *Angew. Chem.* **2022**, *134*, e202211307.

[98] Zhong, J. J.; Liang, Z. H.; Liu, N.; Xiang, Y. C.; Yan, B.; Zhu, F. Y.; Xie, X.; Gui, X. C.; Gan, L. Y.; Yang, H. B. et al. Engineering symmetry-breaking centers and d-orbital modulation in triatomic catalysts for zinc-air batteries. *ACS Nano* **2024**, *18*, 5258–5269.

[99] Deng, D. J.; Qian, J. C.; Liu, X. Z.; Li, H. P.; Su, D.; Li, H. N.; Li, H. M.; Xu, L. Non-covalent interaction of atomically dispersed Cu and Zn pair sites for efficient oxygen reduction reaction. *Adv. Funct. Mater.* **2022**, *32*, 2203471.

[100] Yu, D. S.; Ma, Y. C.; Hu, F.; Lin, C. C.; Li, L. L.; Chen, H. Y.; Han, X. P.; Peng, S. J. Dual-sites coordination engineering of single atom catalysts for flexible metal-air batteries. *Adv. Energy Mater.* **2021**, *11*, 2101242.

[101] Hou, C. C.; Wang, H. F.; Li, C. X.; Xu, Q. From metal-organic frameworks to single/dual-atom and cluster metal catalysts for energy applications. *Energy Environ. Sci.* **2020**, *13*, 1658–1693.

[102] Wang, Z.; Jin, X. Y.; Zhu, C.; Liu, Y. P.; Tan, H.; Ku, R.; Zhang, Y. Q.; Zhou, L. J.; Liu, Z.; Hwang, S. J. et al. Atomically dispersed Co_2–N_6 and Fe–N_4 costructures boost oxygen reduction reaction in both alkaline and acidic media. *Adv. Mater.* **2021**, *33*, 2104718.

[103] Chai, Y. C.; Chen, S. H.; Chen, Y.; Wei, F. F.; Cao, L. R.; Lin, J.; Li, L.; Liu, X. Y.; Lin, S.; Wang, X. D. et al. Dual-atom catalyst with N-colligated Zn_1Co_1 species as dominant active sites for propane dehydrogenation. *J. Am. Chem. Soc.* **2024**, *146*, 263–273.

[104] Chen, X. W.; Peng, M.; Xiao, D. Q.; Liu, H. Y.; Ma, D. Fully exposed metal clusters: Fabrication and application in alkane dehydrogenation. *ACS Catal.* **2022**, *12*, 12720–12743.

[105] Chen, W. M.; Yao, Z.; Chen, W. X.; Shen, Q. K.; Yuan, D. S.; Zhang, C.; Zhu, Y. F.; Liang, H. W.; Wang, Y. G.; Song, W. G. et al. Fully exposed iridium clusters enable efficient hydrogenation of N-heteroarenes. *ACS Catal.* **2023**, *13*, 12153–12162.

[106] Fan, Z. Z.; Luo, R. C.; Zhang, Y. X.; Zhang, B.; Zhai, P. L.; Zhang, Y. T.; Wang, C.; Gao, J. F.; Zhou, W.; Sun, L. C. et al. Oxygen-bridged indium-nickel atomic pair as dual-metal active sites enabling synergistic electrocatalytic CO_2 reduction. *Angew. Chem., Int. Ed.* **2023**, *62*, e202216326.

[107] Jia, Z. M.; Peng, M.; Cai, X. B.; Chen, Y. L.; Chen, X. W.; Huang, F.; Zhao, L. M.; Diao, J. Y.; Wang, N.; Xiao, D. Q. et al. Fully exposed platinum clusters on a nanodiamond/graphene hybrid for efficient low-temperature CO oxidation. *ACS Catal.* **2022**, *12*, 9602–9610.

[108] Zhang, W. X.; Zhang, M. R.; Wang, H. J.; Zhang, W.; Zhang, M. Diatomic Pd catalyst with conjugated backbone for synergistic electrochemical CO_2 reduction. *Nano Res.* **2024**, *17*, 4850–4855.

[109] Xu, Y. X.; Wang, C.; Li, X. Y.; Xiong, L. Q.; Zhang, T. Y.; Zhang, L. Q.; Zhang, Q. H.; Gu, L.; Lan, Y.; Tang J. W. Efficient methane oxidation to formaldehyde via photon-phonon cascade catalysis. *Nat. Sustain.* **2024**, *7*, 1171–1181.

[110] Yue, X. Y.; Cheng, L.; Guan, C.; Liao, Y. L.; Xu, Z. H.; Ostrikov, K. K.; Xiang, Q. J. In-plane palladium and interplanar copper dual single-atom catalyst in bulk-like carbon nitride for cascade CO_2 photoreduction. *Small* **2024**, *20*, 2308767.

[111] Hao, Q.; Zhong, H. X.; Wang, J. Z.; Liu, K. H.; Yan, J. M.; Ren, Z. H.; Zhou, N.; Zhao, X.; Zhang, H.; Liu, D. X. et al. Nickel dual-atom sites for electrochemical carbon dioxide reduction. *Nat. Synth.* **2022**, *1*, 719–728.

[112] Zhang, Q. C.; Liu, D.; Zhang, Y. P.; Guo, Z. L.; Chen, M. P.; Chen, Y. Y.; Jin, B.; Song, Y. Z.; Pan, H. Insight into coupled Ni–Co dual-metal atom catalysts for efficient synergistic electrochemical CO_2 reduction. *J. Energy Chem.* **2023**, *87*, 509–517.

[113] Jiao, J. Q.; Yuan, Q.; Tan, M. J.; Han, X. Q.; Gao, M. B.; Zhang, C.; Yang, X.; Shi, Z. L.; Ma, Y. B.; Xiao, H. et al. Constructing asymmetric double-atomic sites for synergistic catalysis of electrochemical CO_2 reduction. *Nat. Commun.* **2023**, *14*, 6164.
[114] Pei, J. J.; Yang, L.; Lin, J.; Zhang, Z. D.; Sun, Z. Y.; Wang, D. S.; Chen, W. X. Integrating host design and tailored electronic effects of yolk-shell Zn−Mn diatomic sites for efficient CO_2 electroreduction. *Angew. Chem.* **2024**, *136*, e202316123.
[115] Zhao, K.; Nie, X. W.; Wang, H. Z.; Chen, S.; Quan, X.; Yu, H. T.; Choi, W.; Zhang, G. H.; Kim, B.; Chen, J. G. Selective electroreduction of CO_2 to acetone by single copper atoms anchored on N-doped porous carbon. *Nat. Commun.* **2020**, *11*, 2455.
[116] Shao, P.; Zhou, W.; Hong, Q. L.; Yi, L. C.; Zheng, L. R.; Wang, W. J.; Zhang, H. X.; Zhang, H. B.; Zhang, J. Synthesis of a boron-imidazolate framework nanosheet with dimer copper units for CO_2 electroreduction to ethylene. *Angew. Chem., Int. Ed.* **2021**, *60*, 16687–16692.
[117] Xu, H. P.; Rebollar, D.; He, H. Y.; Chong, L. N.; Liu, Y. Z.; Liu, C.; Sun, C. J.; Li, T.; Muntean, J. V.; Winans, R. E. et al. Highly selective electrocatalytic CO_2 reduction to ethanol by metallic clusters dynamically formed from atomically dispersed copper. *Nat. Energy* **2020**, *5*, 623–632.
[118] Sun, Z. Y.; Luo, X.; Shang, H. S.; Wang, Z. D.; Zhang, L.; Chen, W. X. Atomic printing strategy achieves precise anchoring of dual-copper atoms on C_2N structure for efficient CO_2 reduction to ethylene. *Angew. Chem*., in press, DOI: 10.1002/anie.202405778.
[119] Yang, T.; Lin, L.; Lv, X. M.; Yang, H. C.; Feng, H. S.; Huang, Z. L.; Li, J. W.; Pao, C. W.; Hu, Z. W.; Zhan, C. H. et al. Interfacial synergy between the Cu atomic layer and CeO_2 promotes CO electrocoupling to acetate. *ACS Nano* **2023**, *17*, 8521–8529.
[120] Kour, G.; Mao, X.; Du, A. J. A highly efficient conjoined-twin porphyrin-based complex for the electrochemical reduction of CO to ethanol. *ChemNanoMat* **2021**, *7*, 935–941.
[121] Musgrave III, C. B.; Li, Y. Y.; Luo, Z. T.; Goddard, W. A. Dual atom catalysts for rapid electrochemical reduction of CO to ethylene. *Nano Energy* **2023**, *118*, 108966.
[122] Hao, Z. C.; Ma, L. J.; Jia, J. F.; Wu, H. S. Metal-free B_4@gC_3N_4: A potential electrocatalyst for highly selective and efficient conversion of CO to ethanol. *J. Mater. Chem. A* **2023**, *11*, 18365–18374.
[123] Xie, W. F.; Li, H.; Cui, G. Q.; Li, J. B.; Song, Y. K.; Li, S. J.; Zhang, X.; Lee, J. Y.; Shao, M. F.; Wei, M. NiSn atomic pair on an integrated electrode for synergistic electrocatalytic CO_2 reduction. *Angew. Chem.* **2021**, *133*, 7458–7464.
[124] Jiang, J.; Sun, F. F.; Zhou, S.; Hu, W.; Zhang, H.; Dong, J. C.; Jiang, Z.; Zhao, J. J.; Li, J. F.; Yan, W. S. et al. Atomic-level insight into super-efficient electrocatalytic oxygen evolution on iron and vanadium co-doped nickel (oxy)hydroxide. *Nat. Commun.* **2018**, *9*, 2885.
[125] Zhang, S.; Wu, J. H.; Zheng, M. T.; Jin, X.; Shen, Z. H.; Li, Z. H.; Wang, Y. J.; Wang, Q.; Wang, X. B.; Wei, H. et al. Fe/Cu diatomic catalysts for electrochemical nitrate reduction to ammonia. *Nat. Commun.* **2023**, *14*, 3634.
[126] Wang, X. K.; Xu, L. L.; Li, C.; Zhang, C. H.; Yao, H. X.; Xu, R.; Cui, P. X.; Zheng, X. S.; Gu, M.; Lee, J. et al. Developing a class of dual atom materials for multifunctional catalytic reactions. *Nat. Commun.* **2023**, *14*, 7210.
[127] Zhao, Y. S.; Wan, J. W.; Yao, H. Y.; Zhang, L. J.; Lin, K. F.; Wang, L.; Yang, N. L.; Liu, D. B.; Song, L.; Zhu, J. et al. Few-layer graphdiyne doped with sp-hybridized nitrogen atoms at acetylenic sites for oxygen reduction electrocatalysis. *Nat. Chem.* **2018**, *10*, 924–931.
[128] Han, L. L.; Cheng, H.; Liu, W.; Li, H. Q.; Ou, P. F.; Lin, R. Q.; Wang, H. T.; Pao, C. W.; Head, A. R.; Wang, C. H. et al. A single-atom library for guided monometallic and concentration-complex multimetallic designs. *Nat. Mater.* **2022**, *21*, 681–688.
[129] Li, C. G.; Paris, C.; Martínez-Triguero, J.; Boronat, M.; Moliner, M.; Corma, A. Synthesis of reaction-adapted zeolites as methanol-to-olefins catalysts with mimics of reaction intermediates as organic structure-directing agents. *Nat. Catal.* **2018**, *1*, 547–554.
[130] Jeong, H.; Kwon, O.; Kim, B. S.; Bae, J.; Shin, S.; Kim, H. E.; Kim, J.; Lee, H. Highly durable metal ensemble catalysts with full dispersion for automotive applications beyond single-atom catalysts. *Nat. Catal.* **2020**, *3*, 368–375.
[131] Dong, C. Y.; Gao, Z. R.; Li, Y. L.; Peng, M.; Wang, M.; Xu, Y.; Li, C. Y.; Xu, M.; Deng, Y. C.; Qin, X. T. et al. Fully exposed palladium cluster catalysts enable hydrogen production from nitrogen heterocycles. *Nat. Catal.* **2022**, *5*, 485–493.
[132] Liu, Q.; Tang, T.; Tian, Z.; Ding, S.; Wang, L.; Chen, D.; Wang, Z.; Zheng, W.; Lee, H.; Lu, X. et al. A high-performance watermelon skin ion-solvating membrane for electrochemical CO_2 reduction. *Nat. Commun.* **2024**, *15*, 6722.
[133] Deng, Y. C.; Guo, Y.; Jia, Z. M.; Liu, J. C.; Guo, J. Q.; Cai, X. B.; Dong, C. Y.; Wang, M.; Li, C. Y.; Diao, J. Y. et al. Few-atom Pt ensembles enable efficient catalytic cyclohexane dehydrogenation for hydrogen production. *J. Am. Chem. Soc.* **2022**, *144*, 3535–3542.
[134] Chen, Y.; Zhao, J.; Pan, X. L.; Li, L.; Yu, Z. N.; Wang, X. D.; Ma, T. Y.; Lin, S.; Lin, J. Tuning the inter-metal interaction between Ni and Fe atoms in dual-atom catalysts to boost CO_2 electroreduction. *Angew. Chem., Int. Ed*., in press, DOI: 10.1002/anie.202411543.
[135] Zhang, H.; Cao, Y. J.; Sun, M.; Liu, Y.; Wang, Y.; Li, H. R.; Zhang, R. G.; Gu, X. J.; Zeng, S. H. Heterobimetallic praseodymium-nickel active sites with Pr–N_4C_2 and Ni–N_4 moieties enabling synergistic catalysis of CO_2 electroreduction. *Chem. Eng. J.* **2024**, *490*, 151706.
[136] Miao, K.; Wen, J.; Luo, M.; Xiang, D.; Jiang, W.; Duan, D.; Jiang, Z.; Sun, W.; Mei, B.; Xiong, Y. et al. Phosphorus coordination in second shell of single-atom Cu catalyst toward acetate production in CO electroreduction. *Nano Lett.* **2024**, DOI: 10.1021/acs.nanolett.4c03182.
[137] Huang, K.; Li, R.; Qi, H. D.; Yang, S.; An, S. H.; Lian, C.; Xu, Q.; Liu, H. L.; Hu, J. Regulating adsorption of intermediates via the sulfur modulating dual-atomic sites for boosting CO_2RR. *ACS Catal.* **2024**, *14*, 8889–8898.

Acknowledgements

This work was supported by the National Natural Science Foundation of China (22325101, 22171157, 22388102, 223B2902), the National Key R&D Program of China (2023YFA1506801), and the Beijing Natural Science Foundation (Z240027).

Author contributions

J.Y. and D.W. convinced the idea and wrote the paper.

Competing interests

The authors declare no competing interests